

1 **Machine learning-constrained projection of bivariate hydrological**
2 **drought magnitudes and socioeconomic risks**

3 Rutong Liu¹, Jiabo Yin^{1*}, Louise Slater², Shengyu Kang¹, Yuanhang Yang¹, Pan Liu¹, Jiali Guo^{3,4},
4 Xihui Gu⁵, Xiang Zhang⁶, Aliaksandr Volchak⁷

5 ¹State Key Laboratory of Water Resources Engineering and Management, Wuhan University, Wuhan,
6 Hubei, 430072, P.R. China

7 ²School of Geography and the Environment, University of Oxford, Oxford, UK

8 ³Engineering Research Center of Eco-environment in Three Gorges Reservoir Region, Ministry of
9 Education, China Three Gorges University, Yichang, Hubei 443002, China

10 ⁴College of Hydraulic and Environmental Engineering, China Three Gorges University, Yichang,
11 Hubei 443002, China

12 ⁵School of Environmental Studies, China University of Geosciences, Wuhan 430074, China

13 ⁶National Engineering Research Center of Geographic Information System, School of Geography
14 and Information Engineering, China University of Geosciences, Wuhan 430074, China

15 ⁷Engineering Systems and Ecology Faculty, Brest State Technical University, Moskovskaya 267,
16 224017 Brest, Belarus

17

18

19 *Correspondence: Jiabo Yin (jboyn@whu.edu.cn)

20

21 **Abstract**

22 Climate change accelerates the water cycle and alters the spatiotemporal distribution of hydrological
23 variables, thus complicating the projection of future streamflow and hydrological droughts. Although
24 machine learning is increasingly employed for hydrological simulations, few studies have used it to project
25 hydrological droughts, not to mention the bivariate risks of drought duration and severity as well as their
26 socioeconomic effects under climate change. We **developed** a cascade modeling chain to project future
27 bivariate hydrological drought characteristics in 179 catchments over China, using 5 bias-corrected GCM
28 outputs under three shared socioeconomic pathways, five hydrological models and a deep learning model.
29 We **quantified** the contribution of various meteorological variables to daily streamflow by using a random
30 forest model, then employ terrestrial water storage anomalies and a standardized runoff index to evaluate
31 recent changes in hydrologic drought. Subsequently, we **constructed** a bivariate framework to jointly model
32 drought duration and severity by using Copula functions and the most likely realization method. Finally, we
33 **used** this framework to project future risks of hydrological droughts as well as associated exposure of gross
34 domestic product and population. Results **showed** that our hybrid hydrological-deep learning model
35 **achieved** >0.8 Kling-Gupta efficiency in 161 out of 179 catchments. By the late 21st century, bivariate drought
36 risk is projected to double over 60% of catchments, mainly located in Southwest China. Our hybrid model
37 also **projected** substantial GDP and population exposures by increasing bivariate drought risks, suggesting
38 an urgent need to design climate mitigation strategies **toward** a sustainable development pathway.

39 **1 Introduction**

40 In a warming world, the acceleration of the global water cycle is expected to alter the regional and
41 seasonal distribution of key hydrological variables such as precipitation and evapotranspiration (Allan et al.,
42 2020). As precipitation patterns are particularly sensitive to changes in atmospheric forcing and local
43 conditions, precipitation extremes are generally increasing globally, exacerbating spatial heterogeneity of
44 precipitation (Donat et al., 2016; Tabari, 2020). A suite of Shared Socioeconomic Pathways (SSPs) has been
45 proposed to simulate different possible future scenarios of social responses to climate change, and these are
46 employed to investigate the possible effects of long-term climate change (Meinshausen et al., 2020; Zhang
47 et al., 2021). By using the SSP framework, numerous works have indicated that the redistribution of
48 precipitation may lead to the decline of water storage in some regions, and intensify water scarcity in arid
49 regions (Sönmez and Kale, 2018; Woolway et al., 2020; Yao et al., 2023). Under increasing atmospheric
50 greenhouse gases, numerous studies have reported a widespread increase in drought events, even in areas
51 with increasing annual runoff (Dai et al., 2018). The uneven distribution of precipitation and other
52 meteorological elements under climate change complicates predictions of future runoff and drought.

53 China's socioeconomic development, particularly its agricultural sector, is threatened by the rapid
54 intensification of extreme hazards under climate change (Piao et al., 2010). Over the past years, China has
55 been hit by severe drought events which have caused considerable damage to ecosystem productivity and
56 socio-economic growth (Zhai and Zou, 2005; Yin et al., 2023). For instance, one extreme drought in Sichuan
57 Province in 2022 resulted in power shortages and led to economic losses of 669 million dollars. Water
58 shortage is also a key challenge that hinders the sustainable development of the North China Plain (Chen and
59 Yang, 2013). Over the period of 1985-2014, drought accounted for about 19% of economic losses among all
60 meteorological hazards (Chen and Sun, 2019). With continuing global warming, the economic losses from
61 severe drought events might increase by over ten billion US dollars per year by the late 21st century,
62 underscoring the importance of projecting future droughts over China (Lu et al., 2023).

63 Droughts can be triggered by divergent mechanisms, and are thus distinguished according to the type of
64 drought, such as meteorological and hydrological drought (Yihdego et al., 2019). The majority of studies
65 have focused on meteorological droughts, which can then be translated to a hydrological drought, while fewer
66 works have focused on hydrological drought probably due to a lack of measurements like the standardized
67 runoff index (SRI) (Barker et al., 2016; Kumar et al., 2016; Tirivarombo et al., 2018). Furthermore,
68 hydrological droughts are not only affected by the water cycle but also by human interventions, which makes
69 them difficult to accurately be predicted (Wu et al., 2021). Currently, the majority of drought impact
70 assessments focus on the investigation of individual drought variables (i.e., drought duration, severity and
71 intensity, etc.) through univariate probabilistic models and stochastic theory (Myronidis et al., 2018;
72 Byakatonda et al., 2018; Zhang et al., 2022). However, univariate drought analysis cannot accurately describe
73 the probability of drought events, because droughts of either long duration or severe intensity can lead to

74 substantial socio-ecosystem damages (Castle et al., 2014; Udall and Overpeck, 2017). Therefore, the bivariate
75 framework based on Copula functions has been developed for drought projection, compensating for the
76 incompleteness of a single variable analysis (Ayantobo et al., 2017; Nabaei et al., 2019). At present, studies
77 on hydrological drought within a bivariate framework are still lacking. Beyond the choice of approach
78 (univariate or bivariate), the Gravity Recovery and Climate Experiment (GRACE) and GRACE-FO (GRACE
79 Follow-On) satellites now provide two decades of large-scale terrestrial water storage (TWS) data, which
80 captures the water deficit in various forms on land and can be used to monitor droughts (Schmidt et al., 2006).
81 The drought severity index based on TWS (TWS-DSI) can be used to monitor past drought events, which
82 also shows potential advantages in drought warning, forecasting, and projection (Nie et al., 2018; Pokhrel et
83 al., 2021).

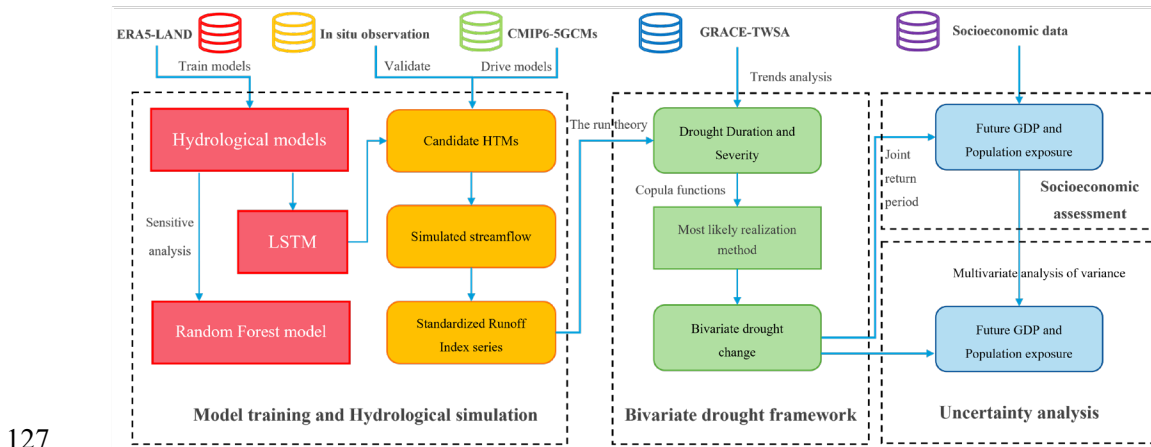
84 In recent decades, many studies have used bias-corrected outputs from Global Climate Models (GCMs)
85 to project future hydrological drought scenarios (e.g., (Ashrafi et al., 2020; Kim et al., 2021; Dixit et al.,
86 2022)). The growing application of machine learning has revealed a high potential for improving the accuracy
87 of hydrological simulation and prediction (Mokhtar et al., 2021). In recent years, many machine learning
88 algorithms have been adopted in drought simulation and produce good performance, such as wavelet neural
89 networks (WNNs) (Xiuji et al., 2022), support vector machines (SVMs) (Zhu et al., 2021) and long short-
90 term memory neural networks (LSTMs) (Dikshit et al., 2021a)). These algorithms can be used to simulate
91 the evolution of future droughts and construct risk maps for drought contingency planning (Rahmati et al.,
92 2020). Among the different models, the LSTMs can effectively simulate short-term and long-term streamflow
93 series, and their performances have been validated at short temporal scales (Dikshit et al., 2021b; Kang et al.,
94 2023).

95 In this study, we **projected** changes in bivariate hydrological drought characteristics (duration and
96 severity) and their associated socioeconomic risks under three SSPs (i.e., SSP1-26, SSP3-70, and SSP5-85)
97 over 179 catchments in China. To achieve this, we **combined** five hydrological models and a deep learning
98 model (i.e., the LSTM), and then **drove** the hybrid models with the five bias-corrected GCMs outputs under
99 Coupled Model Intercomparison Project phase six (CMIP6). Then, we **employed** a machine learning-based
100 framework (i.e., Random Forest, RF model) to quantify the sensitivity of different meteorological variables
101 to daily streamflow. We **employed** the run theory and two drought metrics, the SRI and TWS-DSI, to identify
102 and explore recent changes in drought characteristics. In addition, we **used** Copula functions to build the
103 bivariate model of drought duration and severity during both reference and future periods. After identifying
104 shifts in bivariate drought characteristics based on the most likely realization approach, we **projected** the
105 exposure of gross domestic product (GDP) and population to increasing drought risks in the future. Finally,
106 we **decomposed** the uncertainties arising from different sources by employing the multivariate analysis of
107 variance (MANOVA) method. **This study illustrated the used materials and methods in Section 2 and Section**
108 **3, respectively. We compared SRI and TWS-DSI in assessing drought conditions in Section 4.1. The**
109 **contribution of meteorological factors to simulate streamflow and the calibration of hybrid terrestrial models**
110 **were shown in Section 4.2. The evolution of univariate droughts was projected in Section 4.3. The bivariate**

111 droughts of future scenarios and associated socioeconomic exposures were evaluated in Section 4.4. We
 112 discussed the uncertainty of our analysis and main limitations of this study in Section 5, and finally
 113 summarized our work in Section 6.

114 2. Methodology

115 The workflow of this study is divided into four modules (Figure 1), described briefly below and detailed
 116 in the following sections. In step 1, the hydrological models and LSTM are trained using the ERA5-Land
 117 dataset, and then the output of HMs is used as input to feed the LSTM, thus we build the hybrid terrestrial
 118 models (HTMs). In step 2, the trained HTMs are validated using in situ streamflow observations, then driven
 119 by using the outputs of five GCMs from the CMIP6 to project streamflow and the SRI series. In step 3,
 120 monthly drought characteristics (i.e., drought duration and severity) are defined using run theory and
 121 combined with Copula functions to construct a bivariate drought framework. Future bivariate drought change
 122 is evaluated using the most likely realization method. Meanwhile, the TWS measurements from GRACE
 123 missions are also employed to characterize recent changes in TWS-based droughts, which are also compared
 124 with the hydrological droughts. In step 4, we employ future scenarios of GDP and population alongside our
 125 future drought projections to produce a socioeconomic assessment of drought exposure over China. Finally,
 126 we examine the contribution of uncertainty from different sources in projecting drought change and exposure.



128 **Figure 1. Schematic flowchart of the method, including ML-constrained hydrological simulations, evaluation of**
 129 **bivariate hydrologic drought characteristics and change, and the socioeconomic evaluation to drought exposure**
 130 **under climate change.**

131 2.1 Derivation of 2-meter relative and specific humidity

132 The Clausius–Clapeyron relationship is used to derive saturated vapor pressure (e_s) and air temperature
 133 (T), and is expressed as follows (Koutsoyiannis, 2012):

$$134 \quad e_s(T) = e_0 \exp \left[\left(\frac{1}{T_0} - \frac{1}{T} \right) \frac{L_0}{R_0} \right] \quad (1)$$

135 where T_0 , e_0 , L_0 and R_0 are constants, with a value of 273.16 K, 611 Pa, 2.5×10^6 J kg⁻¹, 461 J kg⁻¹ K⁻¹,
136 respectively;

137 Since near-surface relative humidity (RH) can't be directly obtained from the ERA5-Land dataset, the
138 2m temperature (T_{2m}) and dew-point temperature (T_d) are substituted into equation (1) to calculate RH :

$$139 \quad RH = \frac{e_s(T_d)}{e_s(T_{2m})} = \exp \left[\left(\frac{1}{T_{2m}} - \frac{1}{T_d} \right) \frac{L_0}{R_0} \right] \quad (2)$$

140 Then, the near-surface air pressure (ps) and T_d are used to deduce the specific humidity (SH), which is
141 mathematically expressed as follows (Simmons et al., 1999):

$$142 \quad SH = \frac{0.622 \times e_s(T_d)}{ps - 0.378 e_s(T_d)} \quad (3)$$

143 2.2 Sensitivity analysis on meteorological variables for runoff

144 The RF model is used to calculate the sensitivity to different meteorological variables for runoff,
145 including precipitation (pr), air pressure (ps), surface downwelling shortwave and longwave radiation ($srsds$
146 and $srlsds$), RH , SH , average temperature, maximum and minimum temperature. The contribution of a key
147 variable is derived by using the pre-established model, the perturbed meteorological variable and remaining
148 (non-perturbed) variables (Antoniadis et al., 2021; Green et al., 2020). The percentage change in streamflow
149 is derived from the following equation:

$$150 \quad S_i = \frac{\text{mean}(R_{(i+1SD)} - R_{(all)})}{\text{stdev}(R_{obs})} \times 100\% \quad (4)$$

151 where S_i indicates the sensitivity of streamflow to i^{th} meteorological variable, which are pr , ps , SH , RH , $srlsds$,
152 $srsds$ and temperature; R_{obs} is the observation of streamflow which has units of m³/s; $R_{(i+1SD)}$ is the simulated
153 streamflow by perturbing i by +1 SD; $R_{(all)}$ is the streamflow simulated by all meteorological variables; stdev
154 (R_{obs}) represents the standard deviation of R_{obs} .

155 2.3 Deep learning-constrained hydrological modeling

156 2.3.1 Conceptual hydrological models

157 For preliminary hydrological simulations, we select five hydrological models to represent hydrological
158 characteristics under different environments. The GR4J (Génie Rural à 4 paramètres Journalier) is a lumped
159 model with 4 parameters developed by Perrin et al. (2003). GR4J consists of two water store modules (runoff
160 yielding and routing) and uses daily rainfall and evapotranspiration as inputs to simulate streamflow series
161 (Kunnath-Poovakka and Eldho, 2019). This model has been successfully used to simulate hybrid runoff
162 processes on many continents (Shin and Kim, 2021; Gu et al., 2023). Additionally, we use the temperature-
163 based method (Oudin et al., 2005) to estimate the potential evapotranspiration of the GR4J model.

164 The HBV (Hydrologiska Byråns Vattenbalansavdelning) model was initially developed by the Swedish
165 Meteorological and Hydrological Institute for Hydrological Forecasting (BERGSTRÖM and FORSMAN,
166 1973). This model includes five modules and one transform function to quantify hydrological variables (i.e.,
167 precipitation, snow, soil moisture, runoff, baseflow) (Bergström, 1995). It has been widely employed to
168 simulate streamflow, and it particularly has a good capacity for simulating snowmelt runoff (Kriauciuniene
169 et al., 2013).

170 The HMETs (hydrological model of École de technologie supérieure) model contains 21 parameters
171 and two reservoirs (i.e., the saturated and vadose zones), which makes it simplified and efficient to complete
172 hydrological simulation (Martel et al., 2017). The model can simulate six processes in water cycle, including
173 the accumulation, melts and refreezing of snow, water infiltration and routing, and evapotranspiration (Qi et
174 al., 2020). It has been growly used for streamflow simulation under climate change and has shown great
175 performance (Chen et al., 2018).

176 The SIMHYD (simple lumped conceptual daily rainfall-runoff) model is a daily rainfall-runoff model
177 developed by Porter and McMahon (1975). There are four types of runoff from different sources: impervious
178 areas, infiltration, interflow, and groundwater storage (Chiew et al., 2002). Although the model was
179 developed earlier, it has shown good accuracy in simulating runoff over China (Yu and Zhu, 2015).

180 The XAJ (Xinjiang) model is a hydrological model, which can usually achieve better performance in
181 humid and semi-humid areas than in arid areas (Ren-Jun, 1992). As the model was developed based on the
182 underlying surface of the Yangtze River Basin in China, it is composed of a three-layer evapotranspiration
183 module with four parameters and separates the runoff into four components (i.e., surface water, groundwater,
184 interflow water and flow routing) (Tian et al., 2013). To date, it is widely reported that the XAJ model usually
185 shows the best accuracy in simulating hydrological conditions in China (Hu et al., 2005). However, due to
186 inadequacies in the simulation of arid regions, the results of the XAJ model did not be considered as the best
187 option in northern China.

188 We use the SCE-UA (Shuffled Complex Evolution) approach to maximize the objective function (i.e.,
189 Kling-Gupta efficiency) to optimize these models (Duan et al., 1992). The most complete 20-year observation
190 period is selected to calibrate five models in each watershed. To calibrate the hydrological models, a cross-
191 validation method developed by Arsenault et al. (2017) is used for calibration, which employs the odd years
192 of data to calibrate models, and the even years of data to validate. As catchments are located in different
193 climatic regions, the parameters of models are calibrated for each catchment, which means that the parameters
194 are not universal. Although uncertainties shown by hydrological models are ineradicable, the overall
195 uncertainty is acceptable in the current scale after optimizing five hydrological models for each catchment.

196 **2.3.2 Hybrid scheme of hydrological model and machine learning**

197 Recurrent neural network (RNN) models have had considerable success in hydrological modeling (Cho
198 et al., 2014; Sherstinsky, 2020). However, when considering long input sequences, RNNs struggle to capture
199 the relationships between distant points due to a phenomenon known as “long-term dependencies” (Yu et al.,

200 2019). With the development of deep learning, this problem can be successfully avoided by using LSTMs.

201 An LSTM cell includes input, output and forget gates. The input gate determines which new information
 202 can be stored in the cell state, and the forget gate identifies which information will be discarded from the cell
 203 state. The output gate controls what part of the cell state is selected as the output. The updated cell state is a
 204 combination of the information [retailed](#) and the new information to be added. By using this architecture, the
 205 LSTM can avoid the problem of gradient vanishing or explosion during backpropagation, especially when a
 206 series is long (Gers et al., 2000). The LSTM can be expressed as follows:

$$207 \quad fg_t = \sigma(W_{hf}hs_{t-1} + W_{xf}x_t + b_f) \quad (5)$$

$$208 \quad ig_t = \sigma(W_{hi}hs_{t-1} + W_{xi}x_t + b_{fg}) \quad (6)$$

$$209 \quad \tilde{c}_t = \tanh(W_{hc}hs_{t-1} + W_{xc}x_t + b_c) \quad (7)$$

$$210 \quad c_t = fg_t \cdot c_{t-1} + ig_t \cdot \tilde{c}_t \quad (8)$$

$$211 \quad og_t = \sigma(W_{oh}hs_{t-1} + W_{ox}x_t + b_o) \quad (9)$$

$$212 \quad hs_t = og_t \odot \tanh(c_t) \quad (10)$$

213 where x_t , fg_t , ig_t and og_t are input variables, and forget, input and output gates at time t , respectively; W_i ,
 214 $W_{\tilde{c}}$, W_f and W_o are the weights of each gate; the operator ‘ \odot ’ is the symbol for the dot product of two vectors;
 215 c_t and hs_t are the cell state of the LSTM and the hidden unit at the time t , c_{t-1} and hs_{t-1} at the former time
 216 $t - 1$; \tilde{c}_t is the activation function of hidden layer; b_i , b_f , b_o and b_c are bias items and the; $\sigma(\cdot)$ and $\tanh(\cdot)$
 217 are the sigmoid function and the hyperbolic tangent function, respectively; at the initial moment, cell and
 218 hidden states are set to zero arrays.

219 The hydrological outputs together with other climate variables are used as inputs to feed the LSTM
 220 model (i.e., the HTMs are thus constrained by the LSTM). Because changes in meteorological variables require
 221 some time to converge before they are reflected in the runoff, it is essential to calculate the lag time caused
 222 by the flow convergence for the model. The catchment response lag time d is defined as the time during
 223 which precipitation accumulates in the river to generate runoff for the gauge downstream, and is
 224 mathematically expressed as follows (Berne et al., 2004; Ganguli and Merz, 2019):

$$225 \quad d = 2.51A_d^{0.4} [\text{hrs}] = 0.11A_d^{0.4} [\text{days}] \quad (11)$$

226 where A_d (km²) represents the catchment area; meteorological variables from day $T-d$ to day T are employed
 227 to drive HTMs.

228 We combine the five hydrological models with LSTM to construct five HTMs. To compare the
 229 performance of the HTMs, we use ten HTMs as candidates for streamflow simulation in each catchment. The
 230 calibrated HTMs are then driven by the outputs of five GCMs under each SSP (aggregated to produce a basin

231 average series) during 1985-2100 over 179 catchments to project future daily streamflow.

232 2.4 Drought indexes and run theory

233 The TWS-DSI is employed to measure the degree of terrestrial drought severity (Zhao et al., 2017). It
234 is a dimensionless standardized water storage anomaly index, which can indicate terrestrial drought
235 conditions when below the mean standard value. The TWS-DSI can be mathematically expressed as follows:

$$236 \quad TWS-DSI_{x,y} = (TWS_{x,y} - \overline{TWS}_y) / \sigma_y \quad (12)$$

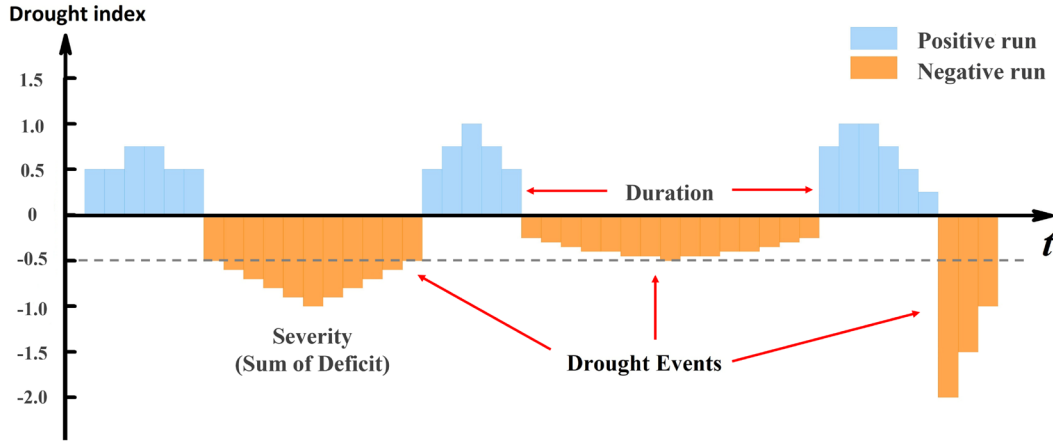
237 where $TWS_{x,y}$ is the TWS at year x and month y ; \overline{TWS}_y and σ_y represent the means and standard deviation
238 of TWS at month y , respectively.

239 The SRI is a measure of the variability of runoff for a given duration based on the percentage of
240 accumulated runoff. (Shukla and Wood, 2008). [The hydrological drought classification and ranges indicated
241 by SRI are shown in Table S1](#). To calculate the SRI, we simulate the retrospective time series of streamflow
242 and fit the sample series to a probability distribution. The SRI is considered to follow a Pearson type-III
243 distribution (Vicente-Serrano et al., 2012), and is calculated as follows:

$$244 \quad SRI = \begin{cases} -\left(r - \frac{c_0 + c_1 r + c_2 r^2}{1 + d_1 r + d_2 r^2 + d_3 r^3}\right) & 0 < F(x) \leq 0.5 \\ r - \frac{c_0 + c_1 r + c_2 r^2}{1 + d_1 r + d_2 r^2 + d_3 r^3} & 0.5 < F(x) \leq 1 \end{cases} \quad (13)$$

245 where $r = \sqrt{\ln \left[\frac{1}{F(x)^2} \right]}$; $F(x)$ is the cumulative probability density of SRI; c_0, c_1, c_2, d_1, d_2 and d_3 are
246 the empirical constants, taken as 2.516, 0.803, 0.010, 1.433, 0.189, 0.001, separately.

247 After calculating the two drought indexes, the degree of water deficit can be determined according to
248 the Grades of Meteorological Drought and the previous classification (Dikici, 2020). Table S1 presents the
249 drought classification and thresholds used for identifying drought degrees. The run theory is employed to
250 obtain characteristics of drought events from the time series (Yevjevich, 1967). When the drought index is
251 below the mild drought (i.e., ≤ -0.5 drought index), a drought event is detected (Figure 2), and then the drought
252 duration and drought severity are extracted.



253

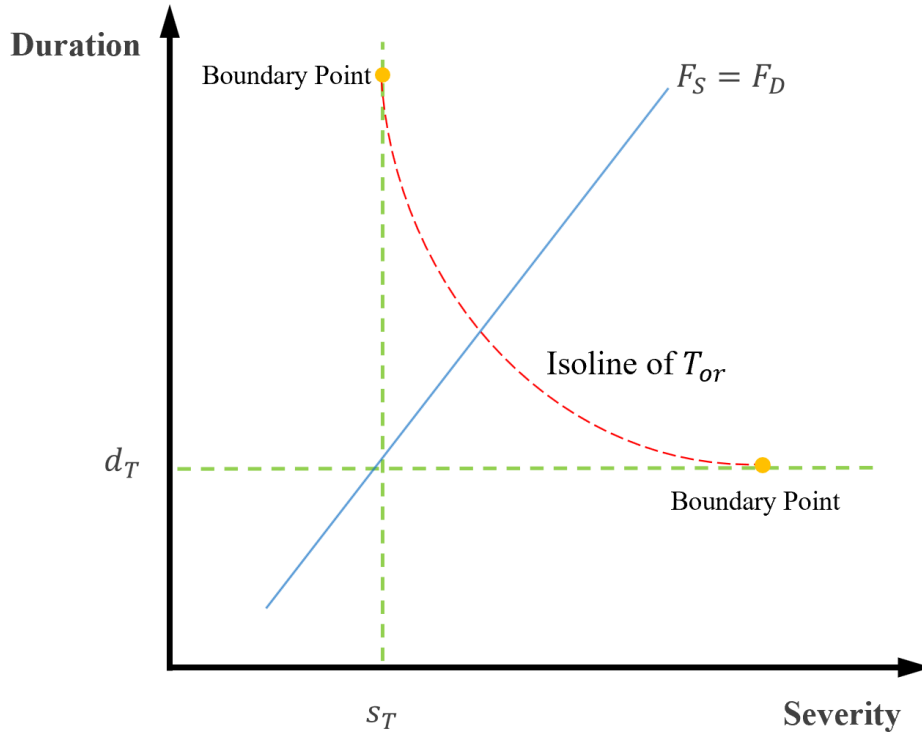
254 **Figure 2. Drought duration and severity identification based on run theory, where -0.5 denotes the drought**
 255 **threshold (grey dash line).**

256 **2.5 Socioeconomic exposure assessments based on the Copulas and most likely realization**

257 After extracting the drought duration (D) and severity (S), we fit their marginal distributions with seven
 258 distributions shown in Table S2. The OR case (i.e., a bivariate drought event is identified with either a high
 259 severity or long duration) of the joint return period (JRP) under a Copula-based framework is used to quantify
 260 the occurrence of drought events (Yin et al., 2020). The joint distribution of drought duration and severity is
 261 constructed by using a Copula function, which is valuable for describing correlated hydrological variables
 262 (Li, 1999). Unlike univariate drought frequency analysis, the JRP within a bivariate framework can be
 263 represented by an isoline, which contains infinite combinations of multivariate variables. It is important for
 264 risk assessments to select a representative combination along the isoline. Previous studies have typically
 265 selected joint design values according to the same frequency hypothesis, but this approach lacks a statistical
 266 basis and poorly describes the physical characteristics of droughts (Yin et al., 2018). In this paper, the joint
 267 probability density is used to optimize the most likely realization, which is mathematically expressed as
 268 follows:

269
$$\left\{ \begin{array}{l} (d^*, s^*) = \arg \max f(d, s) = c[F_d, F_s] \cdot f_d \cdot f_s \\ C[F_d, F_s] = 1 - \mu / T_{or} \\ c[F_d, F_s] = \frac{dC(F_d, F_s)}{d(F_d)d(F_s)} \end{array} \right. \quad (14)$$

270 where $c[F_d, F_s]$ is the Copula probability density function; f_d and f_s are the fitted probability density
 271 functions of D and S , respectively; F_d and F_s are the marginal distribution of D and S , respectively; (d^*, s^*)
 272 is the most likely realization under a given JRP T_{or} ; μ is the mean inter-arrival time between two
 273 consecutive droughts.



274 **Figure 3. Joint distribution of drought duration and severity under a critical T_{or} . The green lines are two arbitrary**
 275 **values of duration and severity. The red line is the isoline line of two variables under a critical T_{or} , and the blue**
 276 **line denotes the traditional equal-frequency assumption.**
 277

278
 279 Socioeconomic exposure has previously been defined as ranging from 0 to 100% in the future period
 280 (Gu et al., 2020a), but dynamically shifting climate risks cannot be represented under this static definition.
 281 Here, the socioeconomic exposure is defined by considering the shift in JRP, and is expressed at the catchment
 282 scale as follows:

$$283 \quad E_{POP} = \frac{T_h I(T_h - T_f)}{T_f A_d} \times POP \quad (15)$$

$$284 \quad E_{GDP} = \frac{T_h I(T_h - T_f)}{T_f A_d} \times GDP \quad (16)$$

285 where E_{POP} and E_{GDP} denote the population and GDP exposure; T_h and T_f denote the historical and future
 286 JRP, respectively; $I(\cdot)$ denotes the controlling function, which is 1 when $T_h - T_f > 0$, or 0 when $T_h - T_f \geq 0$
 287 is recorded; POP (GDP) denotes the population (GDP) of a given catchment in the future climate.

288 2.6 Quantifying the uncertainty contributed by different sources

289 Uncertainties in the future drought projections can arise from the SSPs, GCMs and HTMs. During both
 290 historical (1985-2014) and future periods (2071-2100), the combination of 3 SSPs, 5 GCMs and 10 HTMs

291 through the impact modeling chain resulted in 150 hybrid combinations. The overall uncertainty is calculated
 292 from the variance of the future estimated JRP relative to the historical 50-year droughts. To partition the
 293 **uncertainty** from different sources of data and their interaction effects, the MANOVA is used and expressed
 294 as follows (Weinfurt, 1995):

$$295 \quad \Delta y_{x,y,z} = M + S_x + G_y + H_z + I_{x,y,z} \quad (17)$$

296 where M denotes the mean change of all indicators in models; S_x , G_y and H_z denote the impact on
 297 indicators of the x^{th} SSP, y^{th} GCM and z^{th} HTM, respectively; $I_{i,j,k}$ is the overall impact arising from the
 298 interactions of different sources. The overall variance V is then expressed as follows:

$$299 \quad V = VS + VG + VH + VI_{SG} + VI_{SH} + VI_{GH} + VI_{SGH} \quad (18)$$

300 where VS , VG , VH are the variance from the SSPs, GCMs and HTMs, respectively. VI_{SG} , VI_{SH} , VI_{GH}
 301 and VI_{SGH} denote the variance caused by the coupling between different sources of data. The contribution
 302 of each source to the overall uncertainty is quantified by the variance of each source by the total variance.

303 **3. Data and materials**

304 **3.1 In situ observation dataset**

305 We use a gridded meteorological dataset with $0.5^\circ \times 0.5^\circ$ resolution, including daily temperature
 306 (maximum, minimum and average, $^\circ\text{C}$) and daily precipitation (mm) from 1961 to 2018, provided by the
 307 National Meteorological Bureau of China. The dataset is regarded as the latest gridded meteorological dataset
 308 in China and has been applied to some studies (e.g., Wu et al., 2018; Yin et al., 2021a,b). Meanwhile, we
 309 gathered the daily streamflow of 463 in situ hydrological stations spanning different periods during 1961-
 310 2018. The hydrological stations are densely distributed in East China, while West China has a sparser
 311 distribution. Through rigorous data quality checks, 179 unnested basins with at least 20 years of data are
 312 selected, covering nine major watersheds in China. For more details on streamflow data processing and
 313 catchment screening, please refer to Yin et al. (2021b).

314 **3.2 GRACE/GRACE-FO measurements**

315 Temporal variations in the Earth's gravitational field observed by GRACE satellites have been used to
 316 retrieve TWS data (Tapley et al., 2004). Many international institutes have released the TWS mascon products
 317 at a monthly scale, including the JPL (Jet Propulsion Laboratory of the California Institute of Technology),
 318 the GSFC (Goddard Space Flight Center of NASA), and the CSR (Center for Space Research of the
 319 University of Texas). As these three mascon solutions are produced different spatial resolutions, we produce
 320 blended TWS data based on the average of JPL, GSFC and CSR with $0.5^\circ \times 0.5^\circ$ resolution from 2002 to 2022,

321 and fill the missing data using a linear interpolation approach (Yin et al., 2022).

322 **3.3 ERA5-Land dataset**

323 ERA5-Land is a dataset that consists of a large volume of meteorological variables, including
324 precipitation, temperature and air pressure etc. The spatial resolution of dataset is 9 km and the temporal
325 resolution is one hour (Yilmaz, 2023). Under the latest global reanalysis and the lapse rate correction, the
326 ERA5-Land reanalysis dataset provides a substitute for unavailable observed weather data, by taking the
327 effect of altitude on the spatial scheme of climate variables into consideration (Pelosi et al., 2020). Six
328 variables are used in the study (i.e., pr , ps , T_{2m} , T_{dew} , $srls$, $srsds$) and aggregated to a daily scale from the
329 hourly scale before conducting data analysis.

330 **3.4 Bias-corrected GCM outputs and socioeconomic scenarios**

331 The climate outputs of five GCMs under historical scenario and three SSPs (i.e., SSP1-26, SSP3-70,
332 SSP5-85) under CMIP6 are used to represent climate scenarios. The series of bias-corrected variables have
333 been downscaled to $0.5^\circ \times 0.5^\circ$ resolution from 1850 to 2100 under the Intersectoral Impact Model
334 Intercomparison Project 3b (ISIMIP3b) (Lange, 2019). To reduce the systematical biases of CMIP6 raw
335 outputs, seven variables from the bias-corrected ISMIP3b dataset have been used, namely temperature (daily
336 average, maximum and minimum), pr , ps , $srsds$, $srls$, RH and SH .

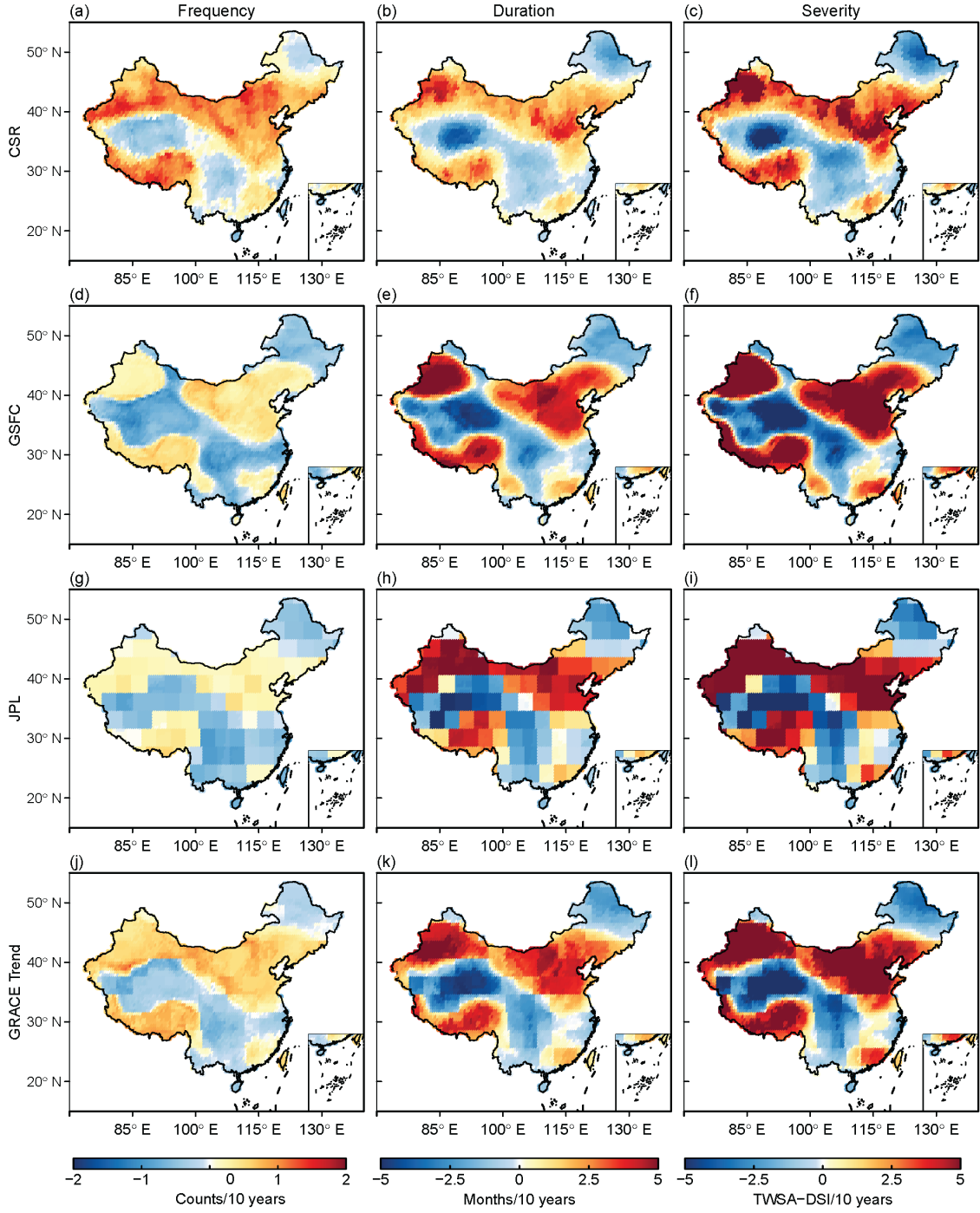
337 Population and GDP data under three SSPs are employed to evaluate the potential socioeconomic risks
338 of drought in a warming world. An open-access population dataset is adopted which takes into consideration
339 the universal two-child policy, the census results and the statistical annual report (Jiang et al., 2017). The
340 economic index from 2010 to 2100 is estimated based on the Cobb-Douglas and Population-Environment-
341 Development model (Jiang et al., 2018). All of the data have been previously used to assess the socio-
342 economic impact of extreme hydrologic hazards (Yin et al., 2022; Yin et al., 2023).

343 **4. Results**

344 **4.1 Observed changes in SRI and TWS based drought**

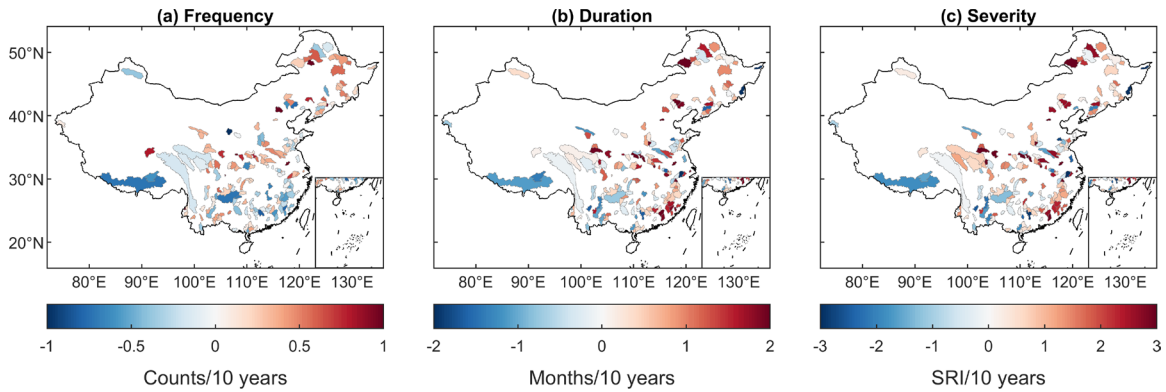
345 As there are insufficient streamflow observations to compute the SRI in northwest China, we also
346 employ the TWS-DSI as a supplement. This approach enriches the variety of water storage or flux being
347 evaluated. Trends in drought characteristics (i.e., frequency, duration and severity) are estimated by using the
348 GRACE/GRACE-FO dataset and observed runoff across China. Figure 4 and Figure 5 show the drought
349 trends based on the TWS-DSI and SRI, respectively. Overall, the two indexes show similar trends in most
350 catchments, suggesting that drought hazards have increased in recent decades. TWS-DSI droughts have
351 increased in 54% of areas, which are mainly located in the Qinghai-Tibet Plateau, the North China Plain and
352 the northwestern Xinjiang Province. Likewise, SRI droughts have increased over 51% of studied catchments,
353 which mainly **dominate** northeastern and southeastern China. The severity of droughts measured by the

354 TWS-DSI index is twice of the hydrological drought, primarily because the TWS-DSI metric incorporates
355 all vertical water fluxes, offering a comprehensive view of shifts in water scarcity. Some locations exhibit
356 discrepancies depending on the index considered. For instance, droughts in the Qinghai-Tibet Plateau and
357 Northeast China show opposite trends. Anomalies in the Qinghai-Tibetan plateau may be explained by the
358 transformation of snowpack melt into surface runoff under the influence of climate change, which helps
359 compensate for the lack of surface water in the area (Stewart, 2009). The discrepancy observed in
360 Northeastern China could potentially be linked to the rise in soil moisture from increased infiltration, which
361 causes a higher proportion of water to be stored within the soil than at the surface, interfering with the
362 quantification of hydrological drought (Wang et al., 2017). Finally, both indicators show a consistent positive
363 drought trend in most areas of China and particularly the North China Plain and Pearl River Basin.



364
 365
 366

Figure 4. Trends in drought frequency, duration and severity based on the TWS-DSI from 2002 to 2022 using three GRACE/GRACE-FO products (a-i) and the blended data (j-l).



367

368

Figure 5. Trends in drought frequency, duration and severity based on SRI over China.

369

4.2 Machine Learning-constrained streamflow simulation and model evaluation

370

371

372

373

374

375

376

377

378

379

380

381

382

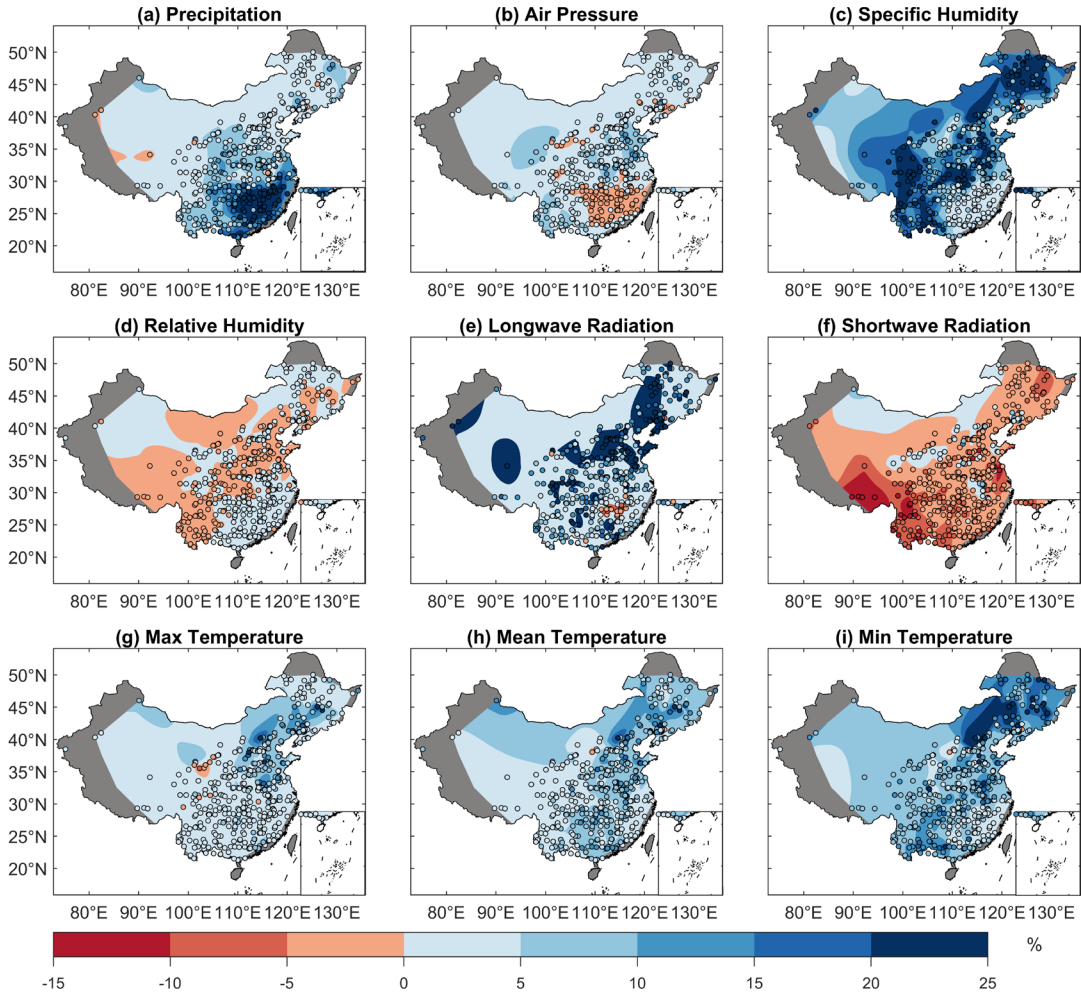
383

384

385

386

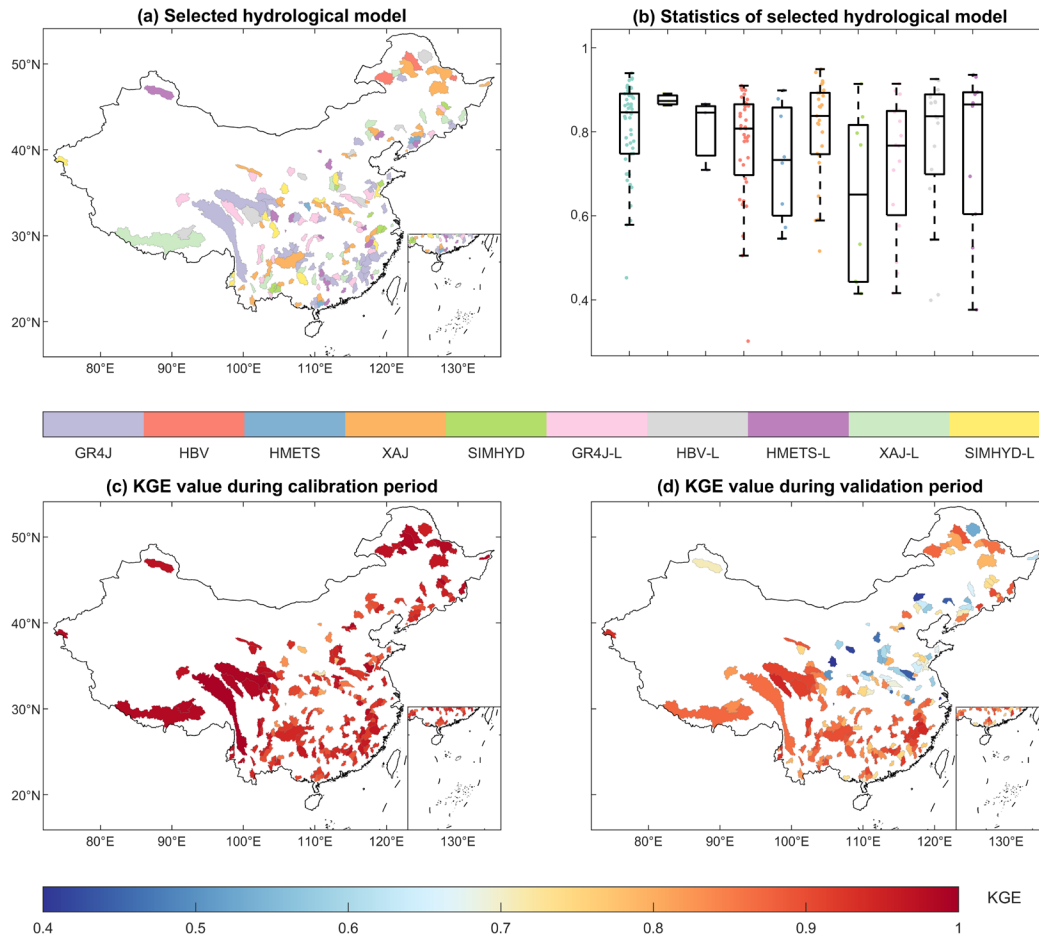
The RF model was used to quantify the sensitivity of streamflow to different meteorological variables (Figure 6). We quantified the sensitivity of seven historical mean meteorological variables (i.e., *pr*, *ps*, *SH*, *RH*, *srls*, *srsds*, temperature) to monthly streamflow in each grid. Due to the sparse number of observation stations in Northwestern China, the reliability of the sensitivity analysis for these regions is lower than that of the dense observed areas. Precipitation typically plays a major role in generating runoff in Southeast China, although *SH* plays the most important role in some regions such as Central, Southwest and Northeast China. Over 30% and 38% of stations show a sensitivity rate of >10% in Western and Northeastern China, respectively. In contrast, *RH* and shortwave radiation have a negative contribution to streamflow; especially shortwave radiation, which has a pronounced negative sensitivity in 394 stations probably due to enhanced evapotranspiration (Ma et al., 2019). In general, *RH* contributes to increasing streamflow over most regions of China, but the opposite effect is observed in 179 stations mainly located in Southwestern China, Yellow River and Huaihe River basins. This is the result of the mutual feedback of water and heat dynamics (i.e., saturated vapor pressure increases with warming and intensifies evaporation, leading to a decrease in surface water), which was also found by Liu et al. (2017). The temperature has a positive contribution to streamflow generation in Northeast China, suggesting a potential mitigation for the deficiency of surface flow. However, there is interactive feedback between hydrological and thermal factors that result in an inability to directly assess the impact of temperature on hydrologic droughts.



387

388 **Figure 6. Sensitivity of meteorological variables to daily streamflow. The figure uses a thin plate smoothing spline**
 389 **method to interpolate the point-based station data (circles). Gray areas indicate missing data.**

390 The performances of simulated streamflow by different HTMs are shown in Figure 7. The model that
 391 has the largest KGE is considered to be the best-performing in each catchment. In Fig 7. (a) and (b), the GR4J
 392 and GR4J-LSTM performed best in 77 out of 179 studied catchments. The median KGE value of GR4J is
 393 higher than 0.83, revealing a superior performance than the other hydrological models. Subsequently, the
 394 XAJ and XAJ-LSTM are the best models in 57 catchments, mainly located in the southern Yangtze River.
 395 Last, the HBV and HBV-LSTM performed best in only 10 catchments, where the streamflow are impacted
 396 by snowfall in plateaus and northern frozen areas. All catchments exhibit KGE values greater than 0.9 during
 397 the calibration period in Figure 7c, showing good performance in simulation. During the validation period,
 398 only 18 catchments have KGE values below 0.6, and most of the catchments have KGE values greater than
 399 0.8 in Figure 7d. In summary, the trained models simulate streamflow well in all the studied catchments.
 400 Additionally, the KGE values in the southern region are generally higher than those in the northern region
 401 during the validation period, which is consistent with previous hydrological simulation works (Gu et al.,
 402 2020b, 2021). This phenomenon may be attributed to the higher dependence of streamflow on rainfall in
 403 South China, which is governed by a humid climate pattern (Zheng et al., 2022).



404

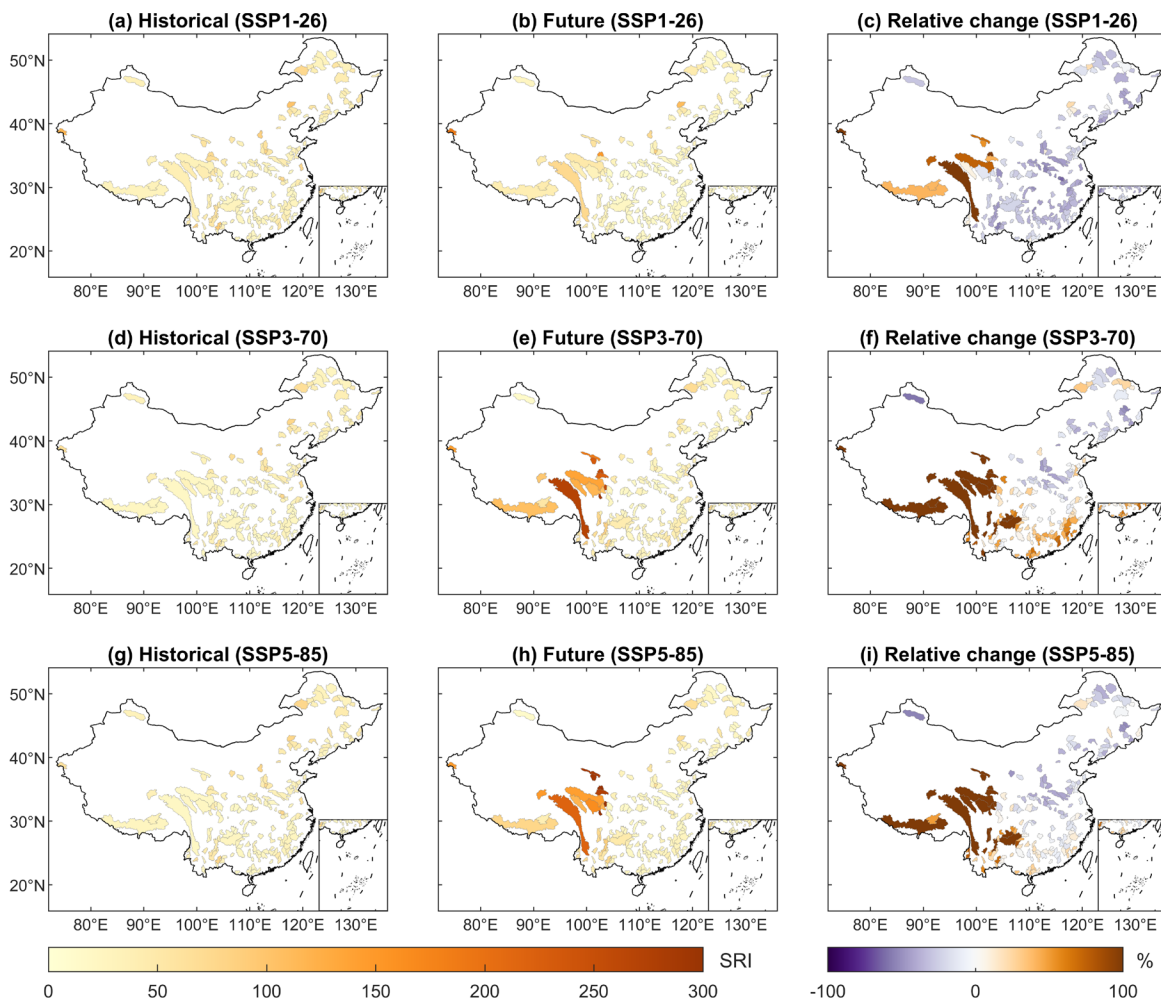
405 **Figure 7. Hydrological simulation performances of all candidate models. (a), The best-performing model with the**
 406 **highest KGE value. (b), Boxplots of all catchments for ten HTMs indicated by KGE values. (c)-(d), The highest**
 407 **KGE values during the calibration (c) and validation (d) period, respectively.**

408 4.3 Projected changes in univariate drought characteristics

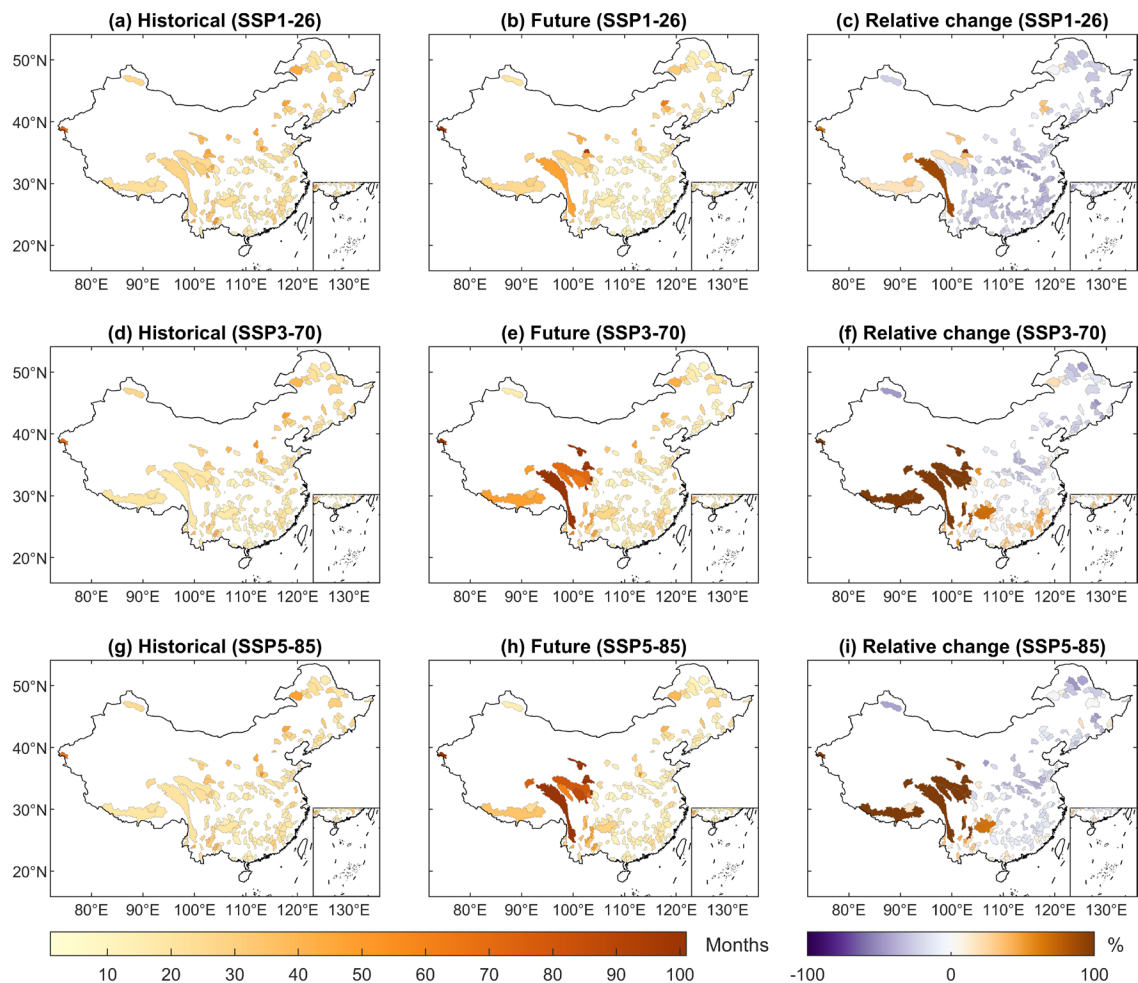
409 We **projected** the future daily runoff series by driving the HTMs with the bias-corrected CMIP6 variables,
 410 and then we **estimated** the monthly SRI to identify drought duration and severity. **Based on the maximum**
 411 **Bayesian Information Criterion (BIC), we selected the best-performing marginal distributions for duration**
 412 **and severity from seven candidate distributions shown in Table S2, based on historical data for each**
 413 **catchment.** Figure 8 and Figure 9 show the multi-model ensemble average severity and duration for the 50-
 414 year historical return period (RP).

415 In western China, we **projected** a significantly increasing drought trend under the three SSPs, which
 416 indicates potential for increased water scarcity and more frequent extreme drought events. In Southeast China,
 417 we **projected** that drought **events** are likely to intensify under SSP3-70 but not under SSP5-85. It is generally
 418 considered that SSP5-85 is accompanied by higher carbon emissions than that of SSP3-70 (O'Neill et al.,
 419 2016). However, future works also take significant action to control the extent of climate change combined
 420 with strong climate policies under SSP5-85 (Fujimori et al., 2017). As a result, there is no deterioration of

421 drought severity with policy interventions, which emphasizes the significance of ensuring the implementation
 422 of climate strategies. In northern China, in contrast, we found that future drought risks are projected to
 423 decrease under the three scenarios, which is possibly related to more moisture convergence from the East
 424 Asian monsoon circulation as the warming climate (Chowdary et al., 2019).



425 **Figure 8. Multi-model ensemble average design severity (dimensionless) under a 50-year RP for three SSPs, and**
 426 **relative changes (%) in 2071-2100 compared to 1985-2014.**
 427

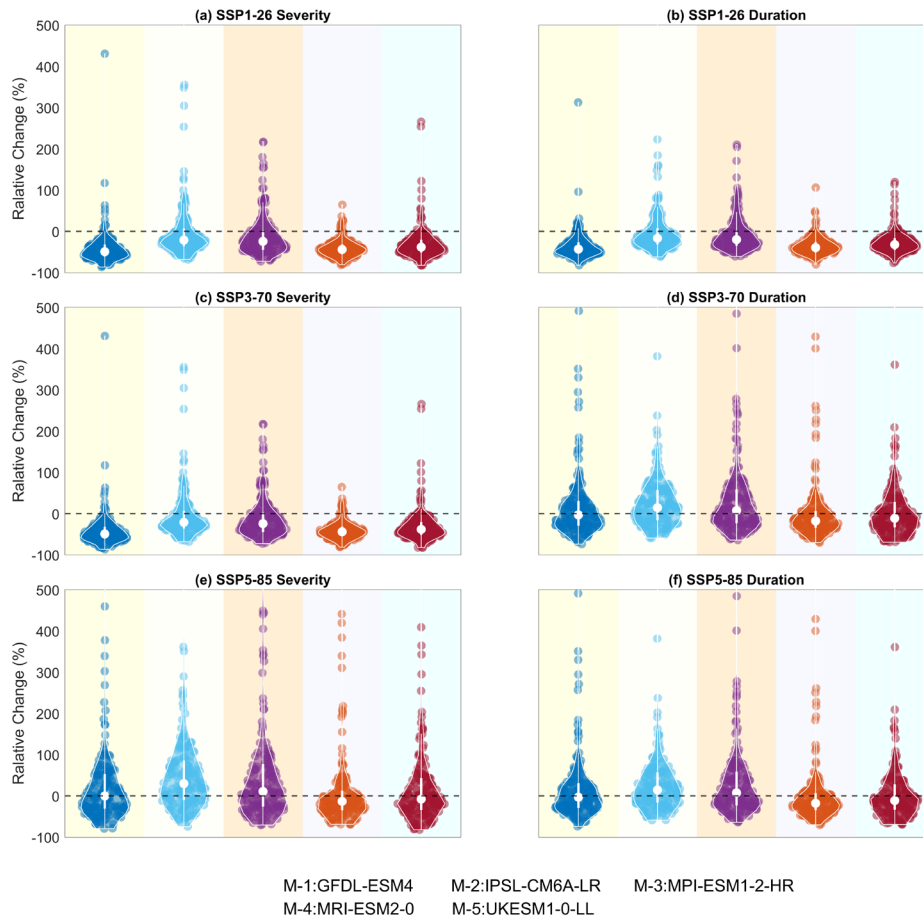


428
429
430

Figure 9. Multi-model ensemble average design duration (months) of the multi-model for a 50-year RP for three SSPs, and relative changes (%) in 2071-2100 compared to 1985-2014.

431
432
433
434
435
436
437
438
439
440

We display the relative change of drought characteristics under 50-year RP for all catchments for five GCMs under the three SSPs using violin plots (Figure 10). For most catchments, the relative change of drought duration and severity is negative. However, the relative change under some scenarios reached a maximum of 400%, highlighting the extreme change of drought. The median relative change of severity based on the IPSL_CM6A_LR under SSP3-70 are 30%, and 22% of catchments have a relative change over 200%, representing the most severe case of drought evolution. Furthermore, the distributions of the projections based on the MPI-ESM1-2-HR, MRI-ESM2-0 and UKESM1-0-LL models are highly skewed and bimodal under SSP3-70 and SSP5-85, revealing substantial spatial heterogeneity across China. Overall, the severity and duration of droughts **slightly** increase in some catchments and have the risk of extreme intensification as global warming.



441

442 **Figure 10. Violin plots of relative changes (%) in severity and duration to the historical drought event with 50-**
 443 **year RP under three SSPs. The white circles are the median values of relative changes.**

444

4.4 Bivariate drought changes and corresponding socioeconomic risks

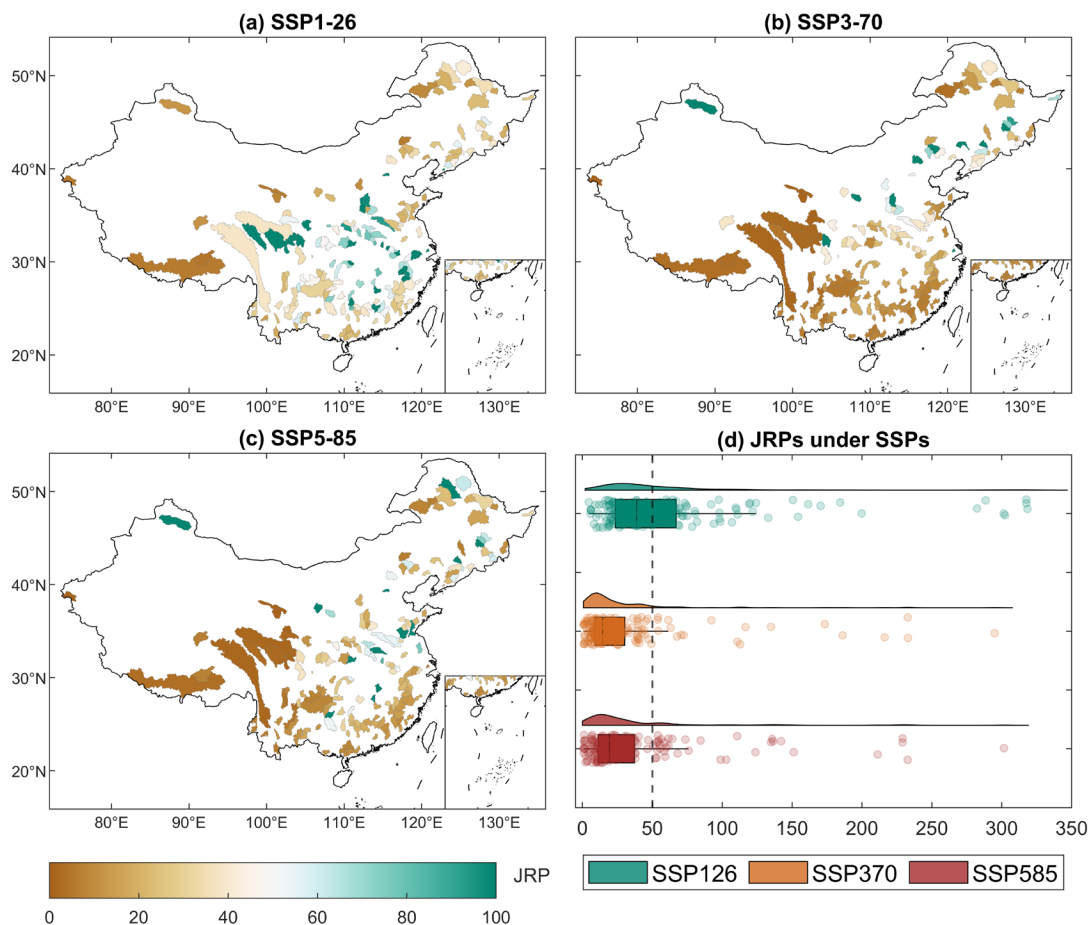
445

To capture the complex dependence structure between drought severity and duration, we use a Copula
 446 function to quantify the bivariate risk of hydrological droughts under climate change. Changes in the JRP of
 447 the historical (1985-2014) drought event with 50-year JRP in the future (2071-2100) period are shown in
 448 Figure 11. The medians of the projected future JRP are 38.78, 14.52 and 19.24 under SSP1-26, SSP3-70 and
 449 SSP5-85, respectively. For 69% and 60% catchments under SSP3-70 and SSP5-85, we find the JRP of the
 450 50-year drought is reduced to less than 25 years in the future period, suggesting that the risk of drought
 451 increases over 2 times in these catchments. Besides, we find a marked increase in the number of catchments
 452 with increased drought risk compared to the univariate drought assessments. The JRP of catchments in
 453 Northeastern and Central China tends to decrease, suggesting higher changes in risks than univariate
 454 assessments. This result is consistent with previous studies (He et al., 2011; Xu et al., 2015), which indicates
 455 that the use of bivariate drought analysis can synthesize the effects of two drought characteristics.

456

Future GDP and population exposed to increasing bivariate drought risk under three scenarios are shown
 457 in Figure 12. The eastern coastal regions have a higher significant economic exposure such as the Huaihe
 458 River Basin, the Yangtze River Basin and the Pearl River Basin, which is consistent with the distribution of

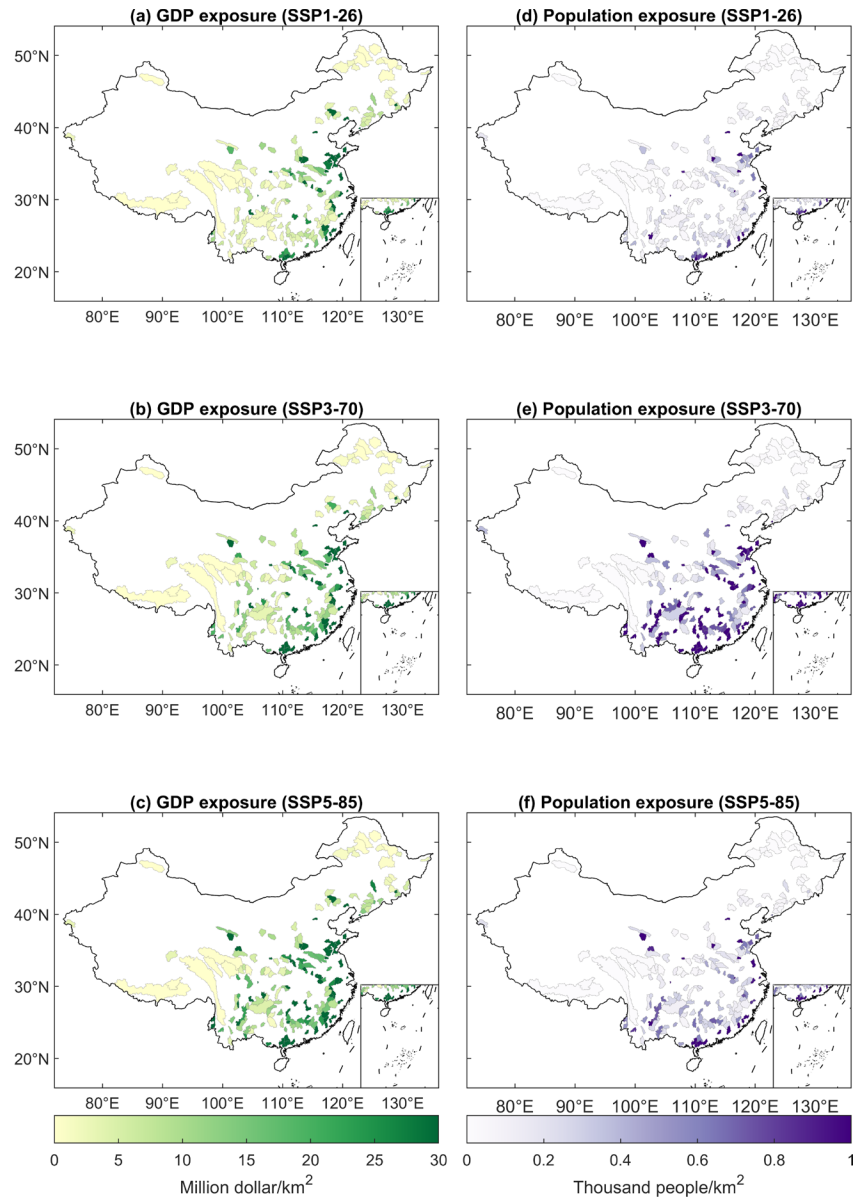
459 economically developed regions in China. The medians of GDP exposure are 5.5, 9.8 and 14.3 million
 460 dollars/km² under three SSPs respectively, which indicates the vulnerability of economic losses to drought
 461 disasters under global warming. The population affected by drought is mainly located in the southern Yangtze
 462 River Basin and the Huaihe River Basin under SSP3-70, as the median exposure is 525 and 205 people/km²
 463 under SSP3-70 and SSP5-85, respectively. This is because the increase in population is higher in the Sichuan,
 464 Guangdong and Zhejiang provinces than in other Chinese provinces under SSP3-70 (Chen et al., 2020).
 465 Overall, the exposure of GDP and population shows large heterogeneity in their sensitivity to different
 466 scenarios, and the distribution of the affected catchments is consistent with economic and social development.



467

468 **Figure 11. The future multi-model ensemble means JRP of the historical drought with a 50-year RP based on**
 469 **the bivariate approach. The future JRPs of 179 catchments under three SSPs are presented in (a)-(c), while (d)**
 470 **displays raincloud plots of the projected JRP under each SSP.**

471



472

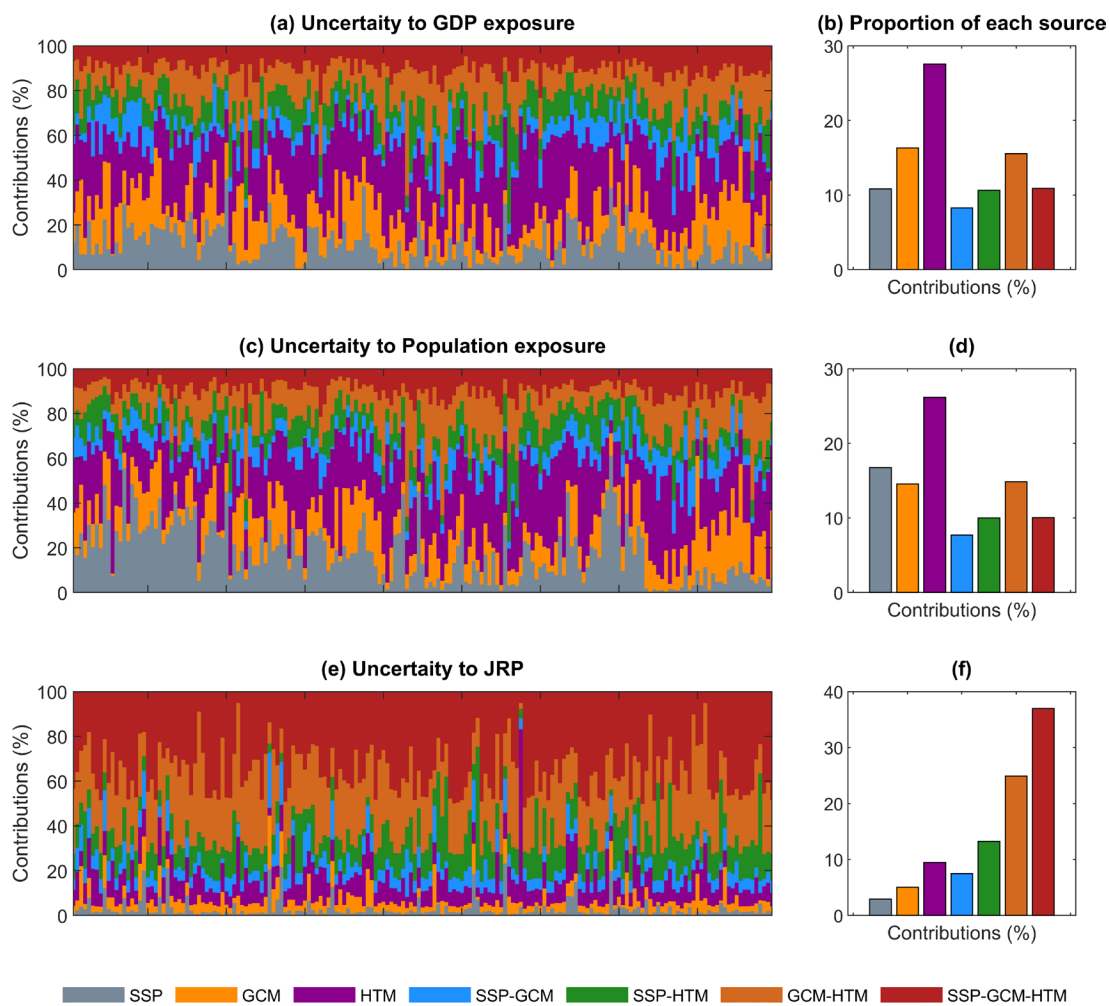
473 **Figure 12. The multi-model ensemble means exposure of GDP (a-c) and population (d-f) to bivariate drought**
 474 **characteristics under different SSPs in the future period.**

475 **5. Discussion**

476 **5.1 Uncertainty decomposition**

477 The overall uncertainty in our projections arises from the different SSPs, GCMs and HTMs as well as
 478 their interactions. We assemble these seven sources using MANOVA (Figure 13). For GDP and POP exposure,
 479 we find HTM is the main source of uncertainty, and contributes 27.55% and 26.14% uncertainty, respectively.
 480 This indicates that the quality of the HTM is important for the accuracy of socioeconomic predictions.
 481 Likewise, the GCM and GCM-HTM provide over 30% of the uncertainty in GDP and population exposures,

482 which indicates the critical importance of bias-corrected GCM outputs for accurate projections. Further, the
 483 contributions of the SSPs to population exposure is 1.5 times than that of GDP exposure, which shows that
 484 the effect of climate change is greater for POP exposure than GDP exposure. In particular, the independent
 485 factors (i.e., SSP, GCM, HTM) contribute over 50% to the uncertainty of GDP and population exposures,
 486 suggesting that GDP and population exposures are less responsive to complex coupling. In contrast, the
 487 coupled factors (i.e., the combination of SSP, GCM or HTM) mainly contribute to the uncertainty of the JRP,
 488 accounting for 82.63% of the overall uncertainty, especially the SSM-GCM-HTM, which accounts for 36.97%
 489 of uncertainty. Finally, the relatively low contribution of the choice of SSP, SSP-GCM and SSP-HTM to JRP
 490 uncertainty indicates that the future risk projection uncertainty is relatively stable in future risk projections



491
 492 **Figure 13. The fractional uncertainty contributions of all sources to the GDP exposure, population exposure, and**
 493 **JRP estimate for all 179 catchments (a, c, e) and the average fractional contribution of each source (b, d, f).**

494 5.2 Limitations and future work

495 The uncertainty caused by the underlying surface situation and the coupling relationships behind
 496 interrelated variables remains unexplained in this study. Therefore, revealing interactions among multisource
 497 data is important to understand how the drivers affect the water cycle under climate change. Here, only five

498 GCM outputs and one in situ observation dataset were used to drive our HTM models. The sparse dataset
499 may undermine the robustness of the approach. Providing a larger number of GCMs and observational data
500 to assemble a more sophisticated model might be an effective approach to improve accuracy and reliability.
501 On the other hand, due to the heterogeneity of different climatic regions in China, we would like to expand
502 hydrological models (e.g., the weather research and forecasting model hydrological modeling system, soil
503 and water assessment tool or the hydrological modules of land surface process models) to reduce uncertainty
504 in future research. Finally, the GDP and population projections cannot well reflect future economic
505 development and population migration, especially the governmental interference in immigration and
506 economic policies. It is better to consider the dynamic impact of human management on socioeconomic
507 development, which is essential for the construction of a more reliable projection framework.

508 **5.3 Suggestions for drought mitigation in China**

509 In order to curb global warming and mitigate the threats of climate change, the Chinese government is
510 striving to reach its carbon peak before 2030, achieve carbon neutrality before 2060, and bolster efforts in
511 disaster reduction (Kundzewicz et al., 2019; Liu et al., 2022b). China has nonetheless experienced several
512 extreme drought events during the past 5 years, threatening the population's health and economic
513 development (Ding and Gao, 2020; Mallapaty, 2022; Liu et al., 2022a). The Intergovernmental Panel on
514 Climate Change (IPCC) has emphasized that projections of future climate trends can equip policymakers
515 with the scientific insight needed to navigate the challenges of climate change (Pörtner et al., 2022). The
516 results of this study aim to alert policymakers to drought risk in Southwestern China which was just hit by
517 severe drought events and expected to significantly intensify with climate change. We strongly highlight the
518 importance of strictly implementing carbon emission reduction initiatives and developing prevention
519 programs to limit potential drought losses. Preserving local ecological balance and employing rational use of
520 water resources could be the key to mitigating potential losses from extreme droughts (Sohn et al., 2016;
521 Chang et al., 2019). Although China has constructed hydraulic structures with a total water storage capacity
522 of over 7,064 billion m³, current irrigation facilities need to expand to mitigate the challenge of drought
523 under climate change (Xiao-jun et al., 2012; Cai et al., 2015). In addition, it is also beneficial for
524 policymakers that establish a drought information system to get a comprehensive collection of drought
525 impacts from all potential sectors, which can link the government and research organizations (Wilhite et al.,
526 2007).

527 The Intergovernmental Panel on Climate Change (IPCC) has emphasized that projections of future
528 climate trends can equip policymakers with the scientific insight needed to navigate the challenges of climate
529 change (Pörtner et al., 2022). The results of this study aim to alert policymakers to drought risk in
530 Southwestern China, which is expected to intensify with climate change. Preserving local ecological balance
531 and employing rational use of water resources could be the key in mitigating potential losses from extreme
532 droughts (Sohn et al., 2016; Chang et al., 2019). Finally, this work highlights the importance of strictly
533 implementing carbon emission reduction initiatives and developing prevention programs to limit potential

534 drought losses.

535 **6. Conclusions**

536 In this study, the hybrid LSTM-constrained hydrological models show high accuracy in studied
537 catchments over China, demonstrating that machine learning can effectively constrain the hydrological
538 projections. Projected changes in 50-year bivariate drought characteristics, expressed as a JRP, indicate that
539 the risk of hydrological drought is likely to more than double in over 60% of catchments by the end of the
540 21st century under SSP5-85. The spatial distribution of change reveals that the catchments with severely
541 increased drought risk are mainly located in southwestern China. Notably, the exposure of GDP and
542 population varies greatly across different SSPs. The median GDP exposure under SSP5-85 is 1.5 times that
543 of SSP3-70, but the median population exposure is just 40% that of SSP3-70. The higher population exposure
544 under SSP3-70 can be attributed to rapid population growth. Finally, we find the interaction between multiple
545 sources of data explains more than 80% of the uncertainty in future changes in JRPs, showing the importance
546 of considering the relationships between model components. [Our findings demonstrate that China will face higher drought risks in a warmer future, emphasizing the urgency of implementing strategies to reduce carbon emissions. Our study is insufficient in the revelation of drought hazard drivers and needs to expand datasets and hydrological models to promote the reliability of simulation in future studies. We would also like to take governmental interference of economic and demographic policies into consideration.](#)

551

552 **Data availability**

553

554 The gridded meteorological dataset for China can be obtained from <http://www.cma.gov.cn>. The
555 ISIMIP3b data can be downloaded from <https://data.isimip.org>. The ERA5-Land data can be
556 downloaded from <https://www.ecmwf.int/en/era5-land>. Streamflow simulations used in this study
557 are available at <https://osf.io/fvyse/>.

558 **Acknowledgments**

559 J.Y. acknowledges support from the National Natural Science Foundation of China (Grant NOs.
560 52361145864; 52261145744). L.S. is supported by UKRI (MR/V022008/1). J.G. is supported by the
561 National Natural Science Foundation of China (NO. 52179018). This work is also supported by the
562 Undergraduate Training Programs for Innovation and Entrepreneurship of Wuhan University. The
563 numerical calculations in this paper have been performed on the supercomputing system in the
564 Supercomputing Center of Wuhan University.

565 **Competing interests**

566 At least one of the (co-)authors is a member of the editorial board of Hydrology and Earth System
567 Sciences.

- 569 Allan, R. P., Barlow, M., Byrne, M. P., Cherchi, A., Douville, H., Fowler, H. J., Gan, T. Y., Pendergrass,
570 A. G., Rosenfeld, D., Swann, A. L. S., Wilcox, L. J., and Zolina, O.: Advances in understanding
571 large-scale responses of the water cycle to climate change, *Annals of the New York Academy of*
572 *Sciences*, 1472, 49–75, <https://doi.org/10.1111/nyas.14337>, 2020.
- 573 Antoniadis, A., Lambert-Lacroix, S., and Poggi, J.-M.: Random forests for global sensitivity analysis: A
574 selective review, *Reliability Engineering & System Safety*, 206, 107312, 2021.
- 575 Arsenault, R., Essou, G. R., and Brissette, F. P.: Improving hydrological model simulations with combined
576 multi-input and multimodel averaging frameworks, *Journal of Hydrologic Engineering*, 22, 04016066,
577 2017.
- 578 Ashrafi, S. M., Gholami, H., and Najafi, M. R.: Uncertainties in runoff projection and hydrological drought
579 assessment over Gharezu basin under CMIP5 RCP scenarios, *Journal of Water and Climate Change*,
580 11, 145–163, 2020.
- 581 Ayantobo, O. O., Li, Y., Song, S., and Yao, N.: Spatial comparability of drought characteristics and related
582 return periods in mainland China over 1961–2013, *Journal of Hydrology*, 550, 549–567, 2017.
- 583 Barker, L. J., Hannaford, J., Chiveron, A., and Svensson, C.: From meteorological to hydrological drought
584 using standardised indicators, *Hydrology and Earth System Sciences*, 20, 2483–2505, 2016.
- 585 Bergström, S.: The HBV model, *Computer models of watershed hydrology*, 443–476, 1995.
- 586 BERGSTRÖM, S. and FORSMAN, A.: DEVELOPMENT OF A CONCEPTUAL DETERMINISTIC
587 RAINFALL-RUNOFF MODEL, *Hydrology Research*, 4, 147–170, 1973.
- 588 Berne, A., Delrieu, G., Creutin, J.-D., and Obled, C.: Temporal and spatial resolution of rainfall
589 measurements required for urban hydrology, *Journal of Hydrology*, 299, 166–179, 2004.
- 590 Byakatonda, J., Parida, B. P., Moalafhi, D. B., and Kenabatho, P. K.: Analysis of long term drought
591 severity characteristics and trends across semiarid Botswana using two drought indices, *Atmospheric*
592 *research*, 213, 492–508, 2018.
- 593 Cai, X., Zeng, R., Kang, W. H., Song, J., and Valocchi, A. J.: Strategic Planning for Drought Mitigation
594 under Climate Change, *Journal of Water Resources Planning and Management*, 141, 04015004,
595 [https://doi.org/10.1061/\(ASCE\)WR.1943-5452.0000510](https://doi.org/10.1061/(ASCE)WR.1943-5452.0000510), 2015.
- 596 Castle, S. L., Thomas, B. F., Reager, J. T., Rodell, M., Swenson, S. C., and Famiglietti, J. S.: Groundwater
597 depletion during drought threatens future water security of the Colorado River Basin, *Geophysical*
598 *research letters*, 41, 5904–5911, 2014.
- 599 Chang, J., Guo, A., Wang, Y., Ha, Y., Zhang, R., Xue, L., and Tu, Z.: Reservoir operations to mitigate
600 drought effects with a hedging policy triggered by the drought prevention limiting water level, *Water*
601 *Resources Research*, 55, 904–922, 2019.
- 602 Chen, H. and Sun, J.: Increased population exposure to extreme droughts in China due to 0.5 °C of
603 additional warming, *Environ. Res. Lett.*, 14, 064011, <https://doi.org/10.1088/1748-9326/ab072e>, 2019.
- 604 Chen, J., Li, C., Brissette, F. P., Chen, H., Wang, M., and Essou, G. R.: Impacts of correcting the inter-
605 variable correlation of climate model outputs on hydrological modeling, *Journal of hydrology*, 560,
606 326–341, 2018.
- 607 Chen, Y., Guo, F., Wang, J., Cai, W., Wang, C., and Wang, K.: Provincial and gridded population
608 projection for China under shared socioeconomic pathways from 2010 to 2100, *Scientific Data*, 7, 83,
609 <https://doi.org/10.1038/s41597-020-0421-y>, 2020.
- 610 Chen, Z. and Yang, G.: Analysis of drought hazards in North China: distribution and interpretation, *Nat*
611 *Hazards*, 65, 279–294, <https://doi.org/10.1007/s11069-012-0358-3>, 2013.
- 612 Chiew, F. H. S., Peel, M. C., and Western, A. W.: Application and testing of the simple rainfall-runoff
613 model SIMHYD., *Mathematical models of small watershed hydrology and applications*, 335–367,
614 2002.
- 615 Cho, K., Van Merriënboer, B., Gulcehre, C., Bahdanau, D., Bougares, F., Schwenk, H., and Bengio, Y.:
616 Learning phrase representations using RNN encoder-decoder for statistical machine translation, *arXiv*
617 *preprint arXiv:1406.1078*, 2014.
- 618 Chowdary, J. S., Hu, K., Srinivas, G., Kosaka, Y., Wang, L., and Rao, K. K.: The Eurasian jet streams as
619 conduits for East Asian monsoon variability, *Current Climate Change Reports*, 5, 233–244, 2019.
- 620 Dai, A., Zhao, T., and Chen, J.: Climate Change and Drought: a Precipitation and Evaporation Perspective,
621 *Curr Clim Change Rep*, 4, 301–312, <https://doi.org/10.1007/s40641-018-0101-6>, 2018.

622 Dikici, M.: Drought analysis with different indices for the Asi Basin (Turkey), *Sci Rep*, 10, 20739,
623 <https://doi.org/10.1038/s41598-020-77827-z>, 2020.

624 Dikshit, A., Pradhan, B., and Huete, A.: An improved SPEI drought forecasting approach using the long
625 short-term memory neural network, *Journal of environmental management*, 283, 111979, 2021a.

626 Dikshit, A., Pradhan, B., and Alamri, A. M.: Long lead time drought forecasting using lagged climate
627 variables and a stacked long short-term memory model, *Science of The Total Environment*, 755,
628 142638, 2021b.

629 Ding, T. and Gao, H.: The record-breaking extreme drought in Yunnan Province, Southwest China during
630 spring-early summer of 2019 and possible causes, *Journal of Meteorological Research*, 34, 997–1012,
631 2020.

632 Dixit, S., Atla, B. M., and Jayakumar, K. V.: Evolution and drought hazard mapping of future
633 meteorological and hydrological droughts using CMIP6 model, *Stochastic Environmental Research
634 and Risk Assessment*, 36, 3857–3874, 2022.

635 Donat, M. G., Lowry, A. L., Alexander, L. V., O’Gorman, P. A., and Maher, N.: More extreme
636 precipitation in the world’s dry and wet regions, *Nature Climate Change*, 6, 508–513, 2016.

637 Duan, Q., Sorooshian, S., and Gupta, V.: Effective and efficient global optimization for conceptual rainfall-
638 runoff models, , 28, 1015–1031, 1992.

639 Fujimori, S., Hasegawa, T., Masui, T., Takahashi, K., Herran, D. S., Dai, H., Hijioka, Y., and Kainuma, M.:
640 SSP3: AIM implementation of shared socioeconomic pathways, *Global Environmental Change*, 42,
641 268–283, 2017.

642 Ganguli, P. and Merz, B.: Trends in compound flooding in northwestern Europe during 1901–2014,
643 *Geophysical Research Letters*, 46, 10810–10820, 2019.

644 Gers, F. A., Schmidhuber, J., and Cummins, F.: Learning to forget: continual prediction with LSTM,
645 *Neural Comput*, 12, 2451–71, 2000.

646 Green, J. K., Berry, J., Ciais, P., Zhang, Y., and Gentine, P.: Amazon rainforest photosynthesis increases in
647 response to atmospheric dryness, *Science Advances*, 6, eabb7232, 2020.

648 Gu, L., Chen, J., Yin, J., Sullivan, S. C., Wang, H.-M., Guo, S., Zhang, L., and Kim, J.-S.: Projected
649 increases in magnitude and socioeconomic exposure of global droughts in 1.5 and 2°C
650 warmer climates, *Hydrology and Earth System Sciences*, 24, 451–472, [https://doi.org/10.5194/hess-
651 24-451-2020](https://doi.org/10.5194/hess-24-451-2020), 2020a.

652 Gu, L., Chen, J., Yin, J., Xu, C.-Y., and Zhou, J.: Responses of precipitation and runoff to climate warming
653 and implications for future drought changes in China, *Earth’s Future*, 8, e2020EF001718, 2020b.

654 Gu, L., Yin, J., Zhang, H., Wang, H.-M., Yang, G., and Wu, X.: On future flood magnitudes and estimation
655 uncertainty across 151 catchments in mainland China, *International Journal of Climatology*, 41, E779–
656 E800, 2021.

657 Gu, L., Yin, J., Wang, S., Chen, J., Qin, H., Yan, X., He, S., and Zhao, T.: How well do the multi-satellite
658 and atmospheric reanalysis products perform in hydrological modelling, *Journal of Hydrology*, 617,
659 128920, <https://doi.org/10.1016/j.jhydrol.2022.128920>, 2023.

660 He, B., Lü, A., Wu, J., Zhao, L., and Liu, M.: Drought hazard assessment and spatial characteristics
661 analysis in China, *Journal of Geographical Sciences*, 21, 235–249, 2011.

662 Hu, C., Guo, S., Xiong, L., and Peng, D.: A modified Xinanjiang model and its application in northern
663 China, *Hydrology Research*, 36, 175–192, 2005.

664 Jiang, T., Jing, Z., Cheng, J., Lige, C., Yanjun, W., Hemin, S., Anqian, W., Jinlong, H., Buda, S., and Run,
665 W.: National and provincial population projected to 2100 under the shared socioeconomic pathways in
666 China, *Advances in Climate Change Research*, 13, 128, 2017.

667 Jiang, T., Jing, Z., Li-Ge, C. A. O., Yan-Jun, W., Bu-Da, S. U., Cheng, J., Run, W., and Chao, G. A. O.:
668 Projection of national and provincial economy under the shared socioeconomic pathways in China,
669 *Advances in Climate Change Research*, 14, 50, 2018.

670 Kim, J. H., Sung, J. H., Chung, E.-S., Kim, S. U., Son, M., and Shiru, M. S.: Comparison of Projection in
671 Meteorological and Hydrological Droughts in the Cheongmicheon Watershed for RCP4. 5 and SSP2-
672 4.5, *Sustainability*, 13, 2066, 2021.

673 Koutsoyiannis, D.: Clausius–Clapeyron equation and saturation vapour pressure: simple theory reconciled
674 with practice, *European Journal of physics*, 33, 295, 2012.

675 Kriauciuniene, J., Jakimavicius, D., Sarauskiene, D., and Kaliatka, T.: Estimation of uncertainty sources in
676 the projections of Lithuanian river runoff, *Stochastic Environmental Research and Risk Assessment*,

677 27, 769–784, 2013.

678 Kumar, R., Musuuza, J. L., Van Loon, A. F., Teuling, A. J., Barthel, R., Ten Broek, J., Mai, J., Samaniego,
679 L., and Attinger, S.: Multiscale evaluation of the Standardized Precipitation Index as a groundwater
680 drought indicator, *Hydrology and Earth System Sciences*, 20, 1117–1131, 2016.

681 Kundzewicz, Z., Su, B., Wang, Y., Xia, J., Huang, J., and Jiang, T.: Flood risk and its reduction in China,
682 *Advances in Water Resources*, 130, 37–45, <https://doi.org/10.1016/j.advwatres.2019.05.020>, 2019.

683 Kunnath-Poovakka, A. and Eldho, T. I.: A comparative study of conceptual rainfall-runoff models GR4J,
684 AWBM and Sacramento at catchments in the upper Godavari river basin, India, *J Earth Syst Sci*, 128,
685 33, <https://doi.org/10.1007/s12040-018-1055-8>, 2019.

686 Lange, S.: Trend-preserving bias adjustment and statistical downscaling with ISIMIP3BASD (v1.0),
687 *Geoscientific Model Development*, 12, 3055–3070, <https://doi.org/10.5194/gmd-12-3055-2019>, 2019.

688 Li, D. X.: On default correlation: A copula function approach, Available at SSRN 187289,
689 <https://doi.org/10.2139/ssrn.187289>, 1999.

690 Liu, J., Zhang, Q., Singh, V. P., and Shi, P.: Contribution of multiple climatic variables and human
691 activities to streamflow changes across China, *Journal of Hydrology*, 545, 145–162,
692 <https://doi.org/10.1016/j.jhydrol.2016.12.016>, 2017.

693 Liu, Y., Hu, Z.-Z., Wu, R., and Yuan, X.: Causes and predictability of the 2021 spring southwestern China
694 severe drought, *Advances in Atmospheric Sciences*, 39, 1766–1776, 2022a.

695 Liu, Z., Deng, Z., He, G., Wang, H., Zhang, X., Lin, J., Qi, Y., and Liang, X.: Challenges and opportunities
696 for carbon neutrality in China, *Nat Rev Earth Environ*, 3, 141–155, <https://doi.org/10.1038/s43017-021-00244-x>, 2022b.

698 Lu, R., Xu, K., Chen, R., Chen, W., Li, F., and Lv, C.: Heat waves in summer 2022 and increasing concern
699 regarding heat waves in general, *Atmospheric and Oceanic Science Letters*, 16, 100290,
700 <https://doi.org/10.1016/j.aosl.2022.100290>, 2023.

701 Ma, N., Szilagyi, J., Zhang, Y., and Liu, W.: Complementary-Relationship-Based Modeling of Terrestrial
702 Evapotranspiration Across China During 1982–2012: Validations and Spatiotemporal Analyses,
703 *Journal of Geophysical Research: Atmospheres*, 124, 4326–4351,
704 <https://doi.org/10.1029/2018JD029850>, 2019.

705 Mallapaty, S.: China’s extreme weather challenges scientists studying it, *Nature*, 609, 888, 2022.

706 Martel, J., Demeester, K., Brissette, F., Poulin, A., and Arsenault, R.: HMETS-A simple and efficient
707 hydrology model for teaching hydrological modelling, flow forecasting and climate change impacts,
708 *International Journal of Engineering Education*, 2017.

709 Meinshausen, M., Nicholls, Z. R., Lewis, J., Gidden, M. J., Vogel, E., Freund, M., Beyerle, U., Gessner, C.,
710 Nauels, A., and Bauer, N.: The shared socio-economic pathway (SSP) greenhouse gas concentrations
711 and their extensions to 2500, *Geoscientific Model Development*, 13, 3571–3605, 2020.

712 Mokhtar, A., Jalali, M., He, H., Al-Ansari, N., Elbeltagi, A., Alsafadi, K., Abdo, H. G., Sammen, S. S.,
713 Gyasi-Agyei, Y., and Rodrigo-Comino, J.: Estimation of SPEI meteorological drought using machine
714 learning algorithms, *IEEE Access*, 9, 65503–65523, 2021.

715 Myronidis, D., Ioannou, K., Fotakis, D., and Dörflinger, G.: Streamflow and hydrological drought trend
716 analysis and forecasting in Cyprus, *Water resources management*, 32, 1759–1776, 2018.

717 Nabaei, S., Sharafati, A., Yaseen, Z. M., and Shahid, S.: Copula based assessment of meteorological
718 drought characteristics: regional investigation of Iran, *Agricultural and Forest Meteorology*, 276,
719 107611, 2019.

720 Nie, N., Zhang, W., Chen, H., and Guo, H.: A global hydrological drought index dataset based on gravity
721 recovery and climate experiment (GRACE) data, *Water Resources Management*, 32, 1275–1290,
722 2018.

723 O’Neill, B. C., Tebaldi, C., Van Vuuren, D. P., Eyring, V., Friedlingstein, P., Hurtt, G., Knutti, R.,
724 Krieger, E., Lamarque, J.-F., and Lowe, J.: The scenario model intercomparison project
725 (ScenarioMIP) for CMIP6, *Geoscientific Model Development*, 9, 3461–3482, 2016.

726 Oudin, L., Hervieu, F., Michel, C., Perrin, C., Andréassian, V., Anctil, F., and Loumagne, C.: Which
727 potential evapotranspiration input for a lumped rainfall-runoff model?: Part 2—Towards a simple and
728 efficient potential evapotranspiration model for rainfall-runoff modelling, *Journal of Hydrology*, 303,
729 290–306, 2005.

730 Pelosi, A., Terribile, F., D’Urso, G., and Chirico, G. B.: Comparison of ERA5-Land and UERRA
731 MESCAN-SURFEX reanalysis data with spatially interpolated weather observations for the regional

732 assessment of reference evapotranspiration, *Water*, 12, 1669, 2020.

733 Perrin, C., Michel, C., and Andréassian, V.: Improvement of a parsimonious model for streamflow
734 simulation, *Journal of hydrology*, 279, 275–289, 2003.

735 Piao, S., Ciais, P., Huang, Y., Shen, Z., Peng, S., Li, J., Zhou, L., Liu, H., Ma, Y., Ding, Y., Friedlingstein,
736 P., Liu, C., Tan, K., Yu, Y., Zhang, T., and Fang, J.: The impacts of climate change on water resources
737 and agriculture in China, *Nature*, 467, 43–51, <https://doi.org/10.1038/nature09364>, 2010.

738 Pokhrel, Y., Felfelani, F., Satoh, Y., Boulange, J., Burek, P., Gädeke, A., Gerten, D., Gosling, S. N.,
739 Grillakis, M., and Gudmundsson, L.: Global terrestrial water storage and drought severity under
740 climate change, *Nature Climate Change*, 11, 226–233, 2021.

741 Porter, J. W. and McMahon, T. A.: Application of a catchment model in southeastern Australia, *Journal of*
742 *Hydrology*, 24, 121–134, 1975.

743 Pörtner, H.-O., Roberts, D. C., Poloczanska, E. S., Mintenbeck, K., Tignor, M., Alegría, A., Craig, M.,
744 Langsdorf, S., Löschke, S., and Möller, V.: IPCC, 2022: Summary for policymakers, 2022.

745 Qi, W., Chen, J., Li, L., Xu, C., Li, J., Xiang, Y., and Zhang, S.: A framework to regionalize conceptual
746 model parameters for global hydrological modeling, *Hydrology and Earth System Sciences*
747 *Discussions*, 1–28, <https://doi.org/10.5194/hess-2020-127>, 2020.

748 Rahmati, O., Falah, F., Dayal, K. S., Deo, R. C., Mohammadi, F., Biggs, T., Moghaddam, D. D., Naghibi,
749 S. A., and Bui, D. T.: Machine learning approaches for spatial modeling of agricultural droughts in the
750 south-east region of Queensland Australia, *Science of the Total Environment*, 699, 134230, 2020.

751 Ren-Jun, Z.: The Xinanjiang model applied in China, *Journal of hydrology*, 135, 371–381, 1992.

752 Schmidt, R., Schwintzer, P., Flechtner, F., Reigber, C., Güntner, A., Döll, P., Ramillien, G., Cazenave, A.,
753 Petrovic, S., and Jochmann, H.: GRACE observations of changes in continental water storage, *Global*
754 *and Planetary Change*, 50, 112–126, 2006.

755 Sherstinsky, A.: Fundamentals of recurrent neural network (RNN) and long short-term memory (LSTM)
756 network, *Physica D: Nonlinear Phenomena*, 404, 132306, 2020.

757 Shin, M.-J. and Kim, C.-S.: Component combination test to investigate improvement of the IHACRES and
758 GR4J rainfall–runoff models, *Water*, 13, 2126, 2021.

759 Shukla, S. and Wood, A. W.: Use of a standardized runoff index for characterizing hydrologic drought,
760 *Geophysical research letters*, 35, 2008.

761 Simmons, A. J., Untch, A., Jakob, C., Källberg, P., and Undén, P.: Stratospheric water vapour and tropical
762 tropopause temperatures in Ecmwf analyses and multi-year simulations, , 125, 353–386, 1999.

763 Sohn, J. A., Saha, S., and Bauhus, J.: Potential of forest thinning to mitigate drought stress: A meta-
764 analysis, *Forest Ecology and Management*, 380, 261–273,
765 <https://doi.org/10.1016/j.foreco.2016.07.046>, 2016.

766 Sönmez, A. Y. and Kale, S.: Climate change effects on annual streamflow of Filyos River (Turkey),
767 *Journal of Water and Climate Change*, 11, 420–433, <https://doi.org/10.2166/wcc.2018.060>, 2018.

768 Stewart, I. T.: Changes in snowpack and snowmelt runoff for key mountain regions, *Hydrological*
769 *Processes*, 23, 78–94, <https://doi.org/10.1002/hyp.7128>, 2009.

770 Tabari, H.: Climate change impact on flood and extreme precipitation increases with water availability,
771 *Scientific reports*, 10, 1–10, 2020.

772 Tapley, B. D., Bettadpur, S., Ries, J. C., Thompson, P. F., and Watkins, M. M.: GRACE measurements of
773 mass variability in the Earth system, *science*, 305, 503–505, 2004.

774 Tian, Y., Xu, Y.-P., and Zhang, X.-J.: Assessment of Climate Change Impacts on River High Flows
775 through Comparative Use of GR4J, HBV and Xinanjiang Models, *Water Resources Management*, 27,
776 2871–2888, 2013.

777 Tirivarombo, S., Osupile, D., and Eliasson, P.: Drought monitoring and analysis: standardised precipitation
778 evapotranspiration index (SPEI) and standardised precipitation index (SPI), *Physics and Chemistry of*
779 *the Earth, Parts A/B/C*, 106, 1–10, 2018.

780 Udall, B. and Overpeck, J.: The twenty-first century Colorado River hot drought and implications for the
781 future, *Water Resources Research*, 53, 2404–2418, 2017.

782 Vicente-Serrano, S. M., López-Moreno, J. I., Beguería, S., Lorenzo-Lacruz, J., Azorin-Molina, C., and
783 Morán-Tejeda, E.: Accurate computation of a streamflow drought index, *Journal of Hydrologic*
784 *Engineering*, 17, 318–332, 2012.

785 Wang, Z., Li, J., Lai, C., Zeng, Z., Zhong, R., Chen, X., Zhou, X., and Wang, M.: Does drought in China
786 show a significant decreasing trend from 1961 to 2009?, *Science of The Total Environment*, 579, 314–

787 324, <https://doi.org/10.1016/j.scitotenv.2016.11.098>, 2017.

788 Weinfurt, K. P.: Multivariate analysis of variance, in: Reading and understanding multivariate statistics,
789 American Psychological Association, Washington, DC, US, 245–276, 1995.

790 Wilhite, D. A., Svoboda, M. D., and Hayes, M. J.: Understanding the complex impacts of drought: A key to
791 enhancing drought mitigation and preparedness, *Water Resour Manage*, 21, 763–774,
792 <https://doi.org/10.1007/s11269-006-9076-5>, 2007.

793 Woolway, R. I., Kraemer, B. M., Lenters, J. D., Merchant, C. J., O'Reilly, C. M., and Sharma, S.: Global
794 lake responses to climate change, *Nat Rev Earth Environ*, 1, 388–403, <https://doi.org/10.1038/s43017-020-0067-5>, 2020.

796 Wu, J., Chen, X., Yao, H., and Zhang, D.: Multi-timescale assessment of propagation thresholds from
797 meteorological to hydrological drought, *Science of the Total Environment*, 765, 144232, 2021.

798 Wu, X., Guo, S., Yin, J., Yang, G., Zhong, Y., and Liu, D.: On the event-based extreme precipitation across
799 China: Time distribution patterns, trends, and return levels, *Journal of hydrology*, 562, 305–317, 2018.

800 Xiao-jun, W., Jian-yun, Z., Shahid, S., ElMahdi, A., Rui-min, H., Zhen-xin, B., and Ali, M.: Water
801 resources management strategy for adaptation to droughts in China, *Mitig Adapt Strateg Glob Change*,
802 17, 923–937, <https://doi.org/10.1007/s11027-011-9352-4>, 2012.

803 Xiujia, C., Guanghua, Y., Jian, G., Ningning, M., and Zihao, W.: Application of WNN-PSO model in
804 drought prediction at crop growth stages: A case study of spring maize in semi-arid regions of
805 northern China, *Computers and Electronics in Agriculture*, 199, 107155, 2022.

806 Xu, K., Yang, D., Yang, H., Li, Z., Qin, Y., and Shen, Y.: Spatio-temporal variation of drought in China
807 during 1961–2012: A climatic perspective, *Journal of Hydrology*, 526, 253–264, 2015.

808 Yao, F., Livneh, B., Rajagopalan, B., Wang, J., Crétau, J.-F., Wada, Y., and Berge-Nguyen, M.: Satellites
809 reveal widespread decline in global lake water storage, *Science*, 380, 743–749,
810 <https://doi.org/10.1126/science.abo2812>, 2023.

811 Yevjevich, V. M.: Objective approach to definitions and investigations of continental hydrologic droughts,
812 An, PhD Thesis, Colorado State University. Libraries, 1967.

813 Yihdego, Y., Vaheddoost, B., and Al-Weshah, R. A.: Drought indices and indicators revisited, *Arab J*
814 *Geosci*, 12, 69, <https://doi.org/10.1007/s12517-019-4237-z>, 2019.

815 Yilmaz, M.: Accuracy assessment of temperature trends from ERA5 and ERA5-Land, *Science of The Total*
816 *Environment*, 856, 159182, <https://doi.org/10.1016/j.scitotenv.2022.159182>, 2023.

817 Yin, J., Guo, S., He, S., Guo, J., Hong, X., and Liu, Z.: A copula-based analysis of projected climate
818 changes to bivariate flood quantiles, *Journal of hydrology*, 566, 23–42, 2018.

819 Yin, J., Guo, S., Gu, L., He, S., Ba, H., Tian, J., Li, Q., and Chen, J.: Projected changes of bivariate flood
820 quantiles and estimation uncertainty based on multi-model ensembles over China, *Journal of*
821 *Hydrology*, 585, 124760, 2020.

822 Yin, J., Guo, S., Gu, L., Zeng, Z., Liu, D., Chen, J., Shen, Y., and Xu, C.-Y.: Blending multi-satellite,
823 atmospheric reanalysis and gauge precipitation products to facilitate hydrological modelling, *Journal*
824 *of Hydrology*, 593, 125878, 2021a.

825 Yin, J., Guo, S., Gentine, P., Sullivan, S. C., Gu, L., He, S., Chen, J., and Liu, P.: Does the hook structure
826 constrain future flood intensification under anthropogenic climate warming?, *Water Resources*
827 *Research*, 57, e2020WR028491, 2021b.

828 Yin, J., Guo, S., Yang, Y., Chen, J., Gu, L., Wang, J., He, S., Wu, B., and Xiong, J.: Projection of droughts
829 and their socioeconomic exposures based on terrestrial water storage anomaly over China, *Sci. China*
830 *Earth Sci.*, 65, 1772–1787, <https://doi.org/10.1007/s11430-021-9927-x>, 2022.

831 Yin, J., Gentine, P., Slater, L., Gu, L., Pokhrel, Y., Hanasaki, N., Guo, S., Xiong, L., and Schlenker, W.:
832 Future socio-ecosystem productivity threatened by compound drought–heatwave events, *Nat Sustain*,
833 6, 259–272, <https://doi.org/10.1038/s41893-022-01024-1>, 2023.

834 Yu, B. and Zhu, Z.: A comparative assessment of AWBM and SimHyd for forested watersheds,
835 *Hydrological sciences journal*, 60, 1200–1212, 2015.

836 Yu, Y., Si, X., Hu, C., and Zhang, J.: A Review of Recurrent Neural Networks: LSTM Cells and Network
837 Architectures, *Neural Comput*, 31, 1235–1270, 2019.

838 Zhai, P. M. and Zou, X. K.: Changes in temperature and precipitation and their impacts on drought in
839 China during 1951–2003, *Advances in Climate Change Research*, 1, 16–18, 2005.

840 Zhang, F., Deng, X., Xie, L., and Xu, N.: China's energy-related carbon emissions projections for the
841 shared socioeconomic pathways, *Resources, Conservation and Recycling*, 168, 105456, 2021.

- 842 Zhang, G., Gan, T. Y., and Su, X.: Twenty-first century drought analysis across China under climate
843 change, *Climate Dynamics*, 59, 1665–1685, 2022.
- 844 Zhao, M., A. G., Velicogna, I., and Kimball, J. S.: Satellite Observations of Regional Drought Severity in
845 the Continental United States Using GRACE-Based Terrestrial Water Storage Changes, *Journal of*
846 *Climate*, 30, 6297–6308, <https://doi.org/10.1175/JCLI-D-16-0458.1>, 2017.
- 847 Zheng, J., Wang, H., and Liu, B.: Impact of the long-term precipitation and land use changes on runoff
848 variations in a humid subtropical river basin of China, *Journal of Hydrology: Regional Studies*, 42,
849 101136, 2022.
- 850 Zhu, Q., Luo, Y., Zhou, D., Xu, Y.-P., Wang, G., and Tian, Y.: Drought prediction using in situ and remote
851 sensing products with SVM over the Xiang River Basin, China, *Natural Hazards*, 105, 2161–2185,
852 2021.
- 853